# Horizon 2020

# H2020 LC-SPACE-04-EO-2019-2020

## Copernicus Evolution – Research for harmonised and Transitional-water Observation (CERTO)

# Project Number: 870349

| Deliverable No: D5.1 | | Work Package: 5 | |
|---|---|---|---|
| Date: | 11-JAN-2021 | Contract delivery due date | 31-DEC-2020 |
| Title: | Initial product evaluation | | |
| Lead Partner for Deliverable | HYGEOS | | |
| Author(s): | François Steinmetz, Didier Ramon, HYGEOS | | |
| Dissemination level (PU=public, RE=restricted, CO=confidential) | | | PU |
| Report Status (DR = Draft, FI = FINAL) | | | DR |

# Table of Contents

# 1 Executive Summary

- The first objective of WP5 is to evaluate, inter-compare and validate different atmospheric correction algorithms in transitional waters, and select the best performing one. This report contains a first evaluation of four atmospheric correction algorithms (Polymer, C2RCC, iCOR and ACOLITE). These algorithms are applied to Sentinel-2 (A and B) and Sentinel-3 (A and B) observations. The evaluation is performed in view of improving the state of the art of atmospheric correction in transitional waters, with a focus on the Polymer algorithm, which has already shown very good capacity to monitor the water colour in coastal and inland waters environments (References to existing publications are provided in this report).

- The atmospheric correction aims at separating two components from an image: the water reflectance, and the atmospheric path reflectance: this separation should perfectly decorrelate both components. A series of images is provided for sample scenes over each CERTO case study region, for both Sentinel-2 and Sentinel-3 products, to allow assessment of the main characteristics of each atmospheric correction algorithm, and to visualize the quality of decoupling between those components, which gives insight on the performance of the atmospheric correction.

- A systematic validation of the water reflectance estimated by each algorithm over the AERONET-OC site of Venice, has been performed. This site is chosen for its proximity to the Venice lagoon, but it does not cover well the situations encountered in the case study sites. This validation exercise will be complemented by additional specific in-situ measurements gathered in CERTO: the validation will be updated in deliverable D5.4 (M24). This updated validation will also address the impact of adjacency effect and bathymetry effect (bottom visibility) on the products.

- The validation results show that the Polymer algorithm performs best over the AERONET-OC site of Venice, for both Sentinel-2 MSI and Sentinel-3 OLCI. Both iCOR and ACOLITE use assumptions of spatial homogeneity of the atmosphere across the scene, and are, therefore, more sensitive to atmospheric perturbation by thin clouds, haze, or sun glint.

- The impact of sun glint on Sentinel-2 MSI imagery over the case study scenes is discussed, because due to a systematic revisit geometry of the MSI sensor, some sites can be continuously affected by sun glint over a season.

- Based on this first evaluation, potential improvements of the Polymer algorithm are foreseen.

# 2   Introduction

Atmospheric correction (AC) is a central topic in CERTO, to develop seamless products for assessing water quality, from oceanic to coastal and inland waters. The application of atmospheric correction algorithms over optically and geographically complex regions, involving challenging optical perturbations from bathymetry effect and adjacency effects, raises numerous questions which are still not resolved yet by the scientific community. WP5 aims at addressing this challenge by first evaluating and inter-comparing atmospheric correction algorithms over optically-complex coastal or inland waters, and then improve them to deliver the most reliable possible products to end users.

This report provides a first evaluation of four atmospheric correction algorithms: Polymer, C2RCC, iCOR and ACOLITE. Observations from both Copernicus sensors, Sentinel-2 MSI (A and B) and Sentinel-3 OLCI (A and B), are considered, to maximise the spatio-temporal coverage, and benefit from the excellent data quality of these instruments. There is a particular focus on the Polymer AC in WP5, and specific developments are planned on this algorithm, because it is already implemented in CLMS for lake quality monitoring, and in C3S for monitoring of oceans/seas through the ocean colour Essential Climate Variable.

WP5 will use in-situ data collected in WP3, but these will only be available later in the project, partly due to delays caused by the COVID-19 pandemic. Therefore, the initial evaluation presented here, relies on two methods:

1) Visualization of sample OLCI and MSI products over the case study regions, and in particular the two components produced by each atmospheric correction algorithm: the water and atmospheric components of the signal. Inspection of these images allows to visualize the quality of decoupling between both components, hence giving insight on the performances of each algorithm (section 5).
2) This qualitative evaluation is complemented by a systematic validation of each atmospheric correction algorithm using the AERONET-OC data from the Venice site of Acqua Alta Oceanographic tower (section 6). Even though this site is not representative of all the complex environments encountered in transitional waters, it gives a first insight on the performance of each algorithm. This methodology will be applied easily to new in-situ data as they are available from WP3.

Before the product evaluation itself, the algorithms considered in this WP are presented in section 3, with references to useful papers including validation of Sentinel-2 and Sentinel-3 products over different regions; section 4 discusses the impact of sun glint on MSI imagery.

# 3   Atmospheric correction algorithms

The following atmospheric correction algorithms have been considered for comparison in this project. They have been selected based on their public availability, and the applicability to the MSI and OLCI sensors.

| Algorithm | Principle | OLCI | MSI |
|---|---|---|---|
| **Polymer** | Iterative spectral matching over visible and NIR bands using analytical atmospheric reflectance model<br>www.hygeos.com/polymer | ✓ | ✓ |
| **C2RCC** | Uses Neural Networks to invert the TOA spectrum based on radiative transfer simulations<br>https://step.esa.int/main/download/ | ✓ | ✓ |
| **ACOLITE** | Uses SWIR bands for dark spectrum fitting (DSF)<br>Assumes spatial homogeneity over a scene or sub-scene (image-based only)<br>https://odnature.naturalsciences.be/remsem/software-and-data/acolite | ✗<br>(requires SWIR bands) | ✓ |
| **iCOR** | Focused on land processing<br>Assumes spatial homogeneity over tiles<br>https://remotesensing.vito.be/case/icor | ✓ | ✓ |

**Polymer** [Steinmetz et al. 2011, Steinmetz & Ramon 2018] is an iterative spectral matching algorithm, relying on a simple polynomial-like model for the atmospheric path reflectance, and a semi-analytic model for the water reflectance. It has been designed to work in presence of sun glint, and has been first applied to MERIS, then to various other sensors.

**C2RCC** [Brockmann et al. 2016, Doerffer & Schiller 2007] use a neural network approach, trained on radiative transfer simulations. It has several similarities with Polymer: (1) it is a pixel by pixel algorithm, (2) it uses the full sensor spectrum for atmospheric correction, and (3) it relies on a model of reflectance for the water component.

**ACOLITE** [Vanhellemont 2019] is an image-based algorithm which evaluates the aerosol properties in the NIR and SWIR. This evaluation is based on the dark spectrum fitting (DSF), which uses multiple dark targets in the subscene to construct a "dark spectrum", which is then propagated towards the visible bands.

**iCOR** [Keukelaere et al. 2018] is also image-based, but instead of relying on dark pixel assumption, it inverts the aerosol properties from the spectral variability within a land subset of the product (or can use the aerosol optical thickness as ancillary information). Therefore, iCOR cannot be applied to water-only products.

Due to the assumption of spatial homogeneity across the image, iCOR and Acolite are sensitive to small-scale atmospheric perturbations, like cloud edges, haze, or sun glint (this will be verified later in this report). To avoid outliers, these algorithms are often validated on cloud-free images [Pereira-Sandoval et al. 2019, Renosh et al. 2020].

**Papers relevant to the validation of atmospheric correction algorithms in CERTO**

Several papers have been published, which have evaluated and inter-compared the atmospheric correction algorithms mentioned here.

[Pereira-Sandoval et al. 2019] reported best performance of Polymer and C2RCC compared to reflectance measured in the Valencia region. [Renosh et al. 2020] focussed on extremely turbid waters, and report the best performance of iCOR. Polymer is also validated by [Zhang & Hu 2020], who compared the results with MODIS only, and mention that "The lack of

apparent adjacency effects in POLYMER-retrieved Rrs makes the MSI data even more valuable for estuarine and coastal waters."

An exhaustive validation of Sentinel-2A MSI products, relevant to CERTO, was performed in two optically diverse coastal regions and 13 inland water bodies [Warren et al. 2019]. This paper concluded that C2RCC and Polymer are the best performing algorithms among the six considered (Acolite, C2RCC, iCOR, l2gen, Polymer and Sen2COR).

[Alikas et al. 2020] validated Sentinel-3A products in Estonian inland waters and Baltic sea coastal waters, and concluded that "POLYMER to be most suitable for optically complex waters under study in terms of product accuracy, amount of usable data and also being least influenced by the adjacency effect".
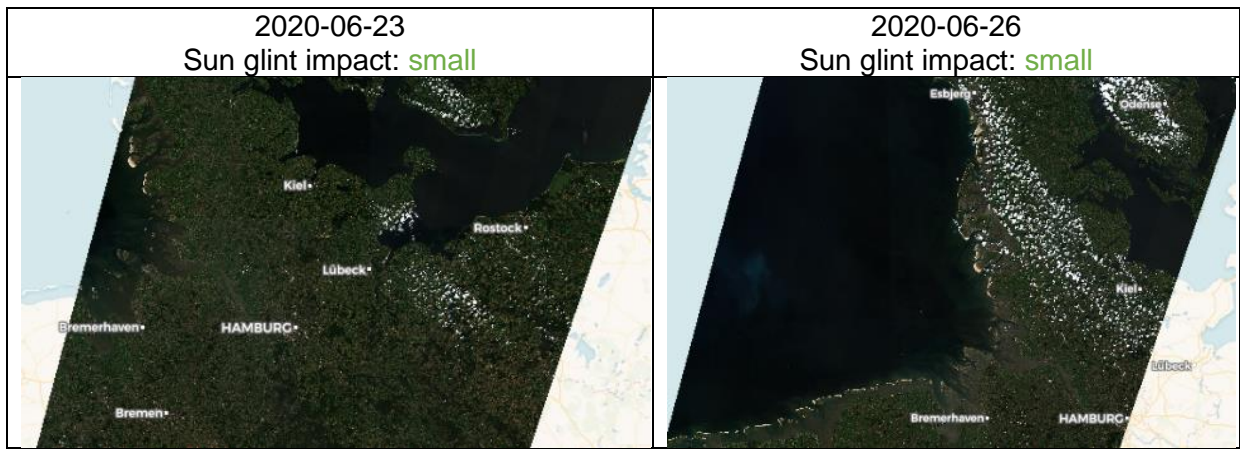
[König et al. 2019] also compared different atmospheric correction algorithms for validating MSI products in the Arctic region. Comparing ACOLITE, ATCOR, iCOR, Polymer, and Sen2Cor, they observed that Polymer was the best performing, and was also insensitive to adjacency effect.

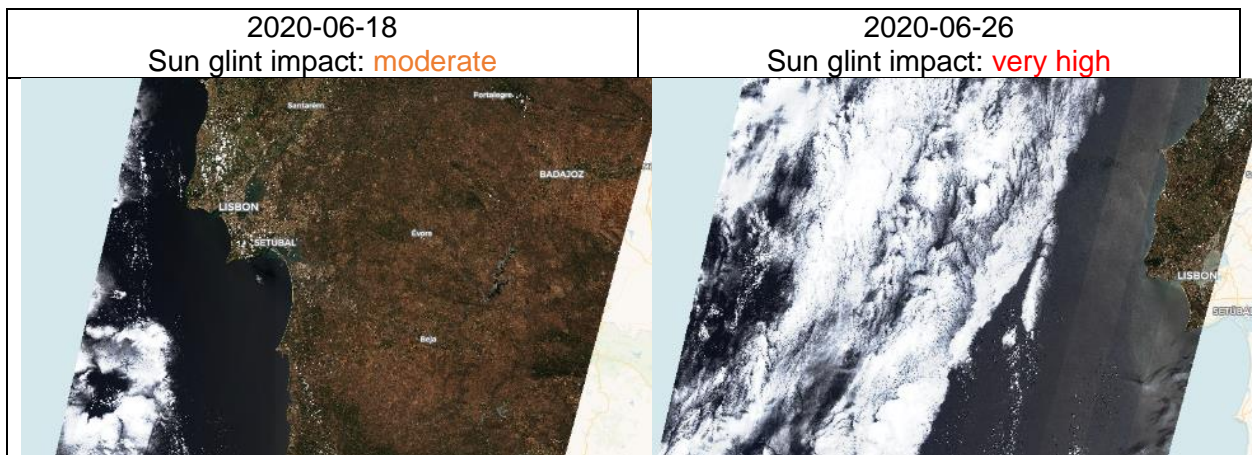# 4 Sun glint: impact over case study sites with MSI

In this section, we discuss how the CERTO case study areas are affected by the sun glint on MSI imagery. Due to the Sentinel-2 orbit and swath, each site is revisited at a limited number of fixed sensor zenith angles, or equivalently, at fixed positions within the MSI swath. At tropical latitudes, sites may only be revisited at a single sensor zenith angle, but at higher latitudes, revisits may occur at several sensor zenith angles. This fact has **an important consequence on the impact of sun glint**, because some sites may be **continuously affected by sun glint over a season** (in boreal summer in the northern hemisphere). The revisit cycles of Sentinel-2A and Sentinel-2B are also identical, therefore, the presence of two satellites does not mitigate the impact of sun glint. This is not true for Sentinel-3 OLCI, for which each site can be revisited at various positions within the swath, therefore, mitigating the impact of sun glint.

Here, we present for each case study site, examples of MSI observations, representing **all possible observation positions** of the case study sites within the MSI swath. These cases illustrate the maximal impact of sun glint, and are, therefore, selected close to the summer solstice. The maximal intensity of the sun glint depends on the possible positions of the site within an MSI swath: it is minimal (and negligible) on the left edge of the swath, moderate in the centre of the swath, and maximal at the right edge of the swath: this is because the Sentinel 2 spacecraft overfly in the morning when the sun is to the east (or right on the images). An example showing the maximal impact of the sun glint across the MSI swath is illustrated in section 3.2.6 (MSI product of 2020-06-19 over the Venice lagoon).
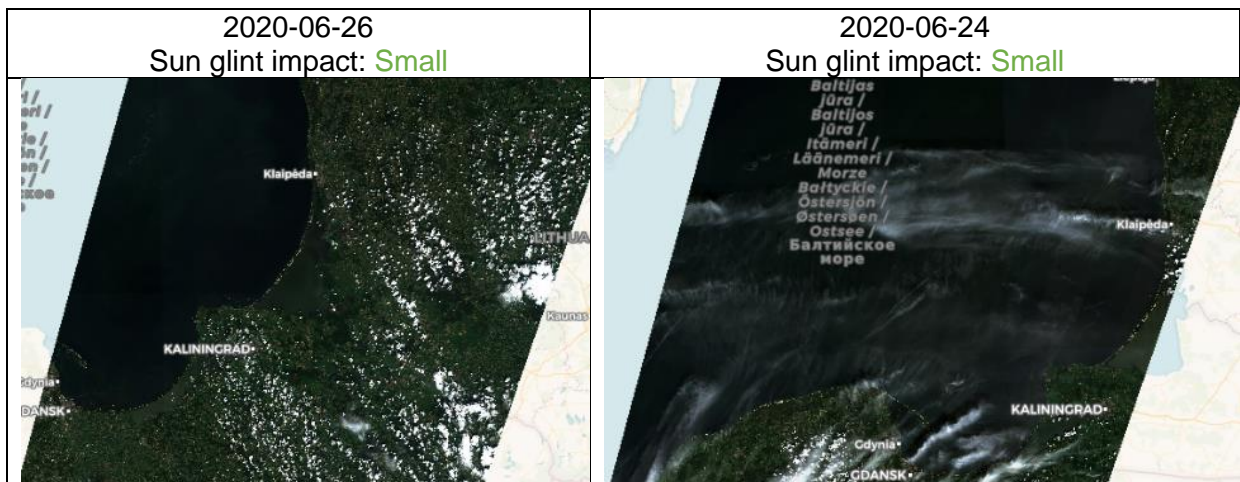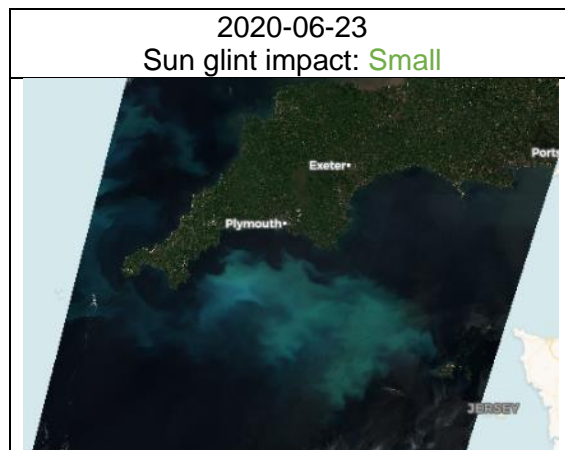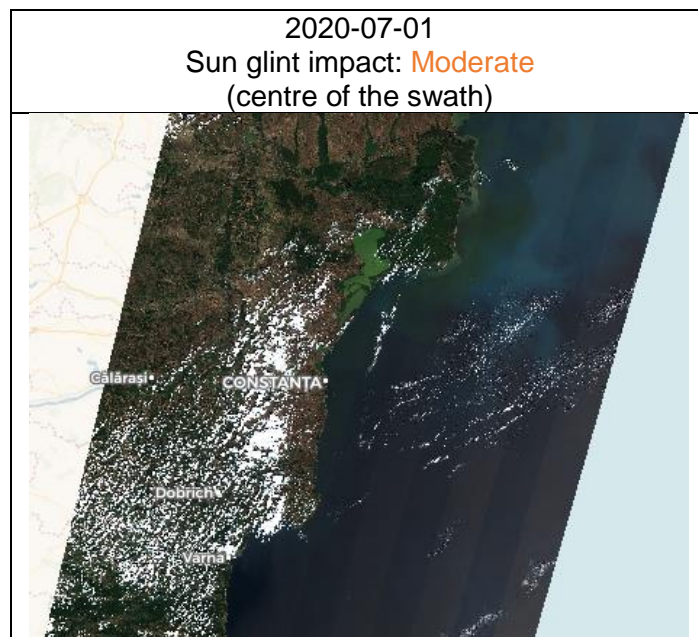
## 4.1 Elbe estuary/German Bight

| 2020-06-23<br>Sun glint impact: small | 2020-06-26<br>Sun glint impact: small |
|---|---|
|  |  |

## 4.2 Tagus Estuary

| 2020-06-18<br>Sun glint impact: moderate | 2020-06-26<br>Sun glint impact: very high |
|---|---|
|  |  |

## 4.3 Curonian lagoon

| 2020-06-26<br>Sun glint impact: Small | 2020-06-24<br>Sun glint impact: Small |
|---|---|
|  |  |

## 4.4 Tamar estuary / Plymouth Sound



2020-06-23
Sun glint impact: Small

## 4.5 Razelm-Sinoe Lagoon System



2020-07-01
Sun glint impact: Moderate
(centre of the swath)

## 4.6  Venice lagoon

| 2020-06-19<br>Sun glint impact: Small but only partial coverage of the lagoon | 2020-06-22<br>Sun glint impact: High |
| --- | --- |
|  |  |
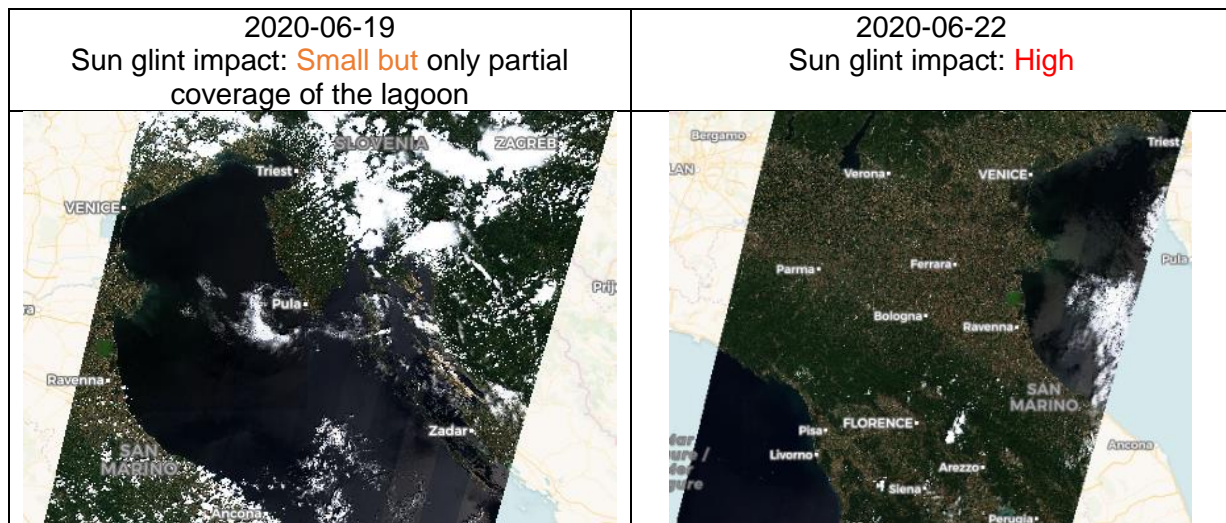
## 4.7  Summary

| Case study site | Impact of sun glint (in summer) | |
| --- | --- | --- |
| | *First observation geometry* | *Second observation geometry* |
| **Elbe estuary** | Small | Small |
| **Tagus estuary** | Moderate | Very high |
| **Curonian lagoon** | Small | Small |
| **Tamar estuary** | Small | - |
| **Razelm-Sinoe Lagoon** | Moderate | - |
| **Venice lagoon** | Small, but only partial coverage | High |

We observed that the most impacted sites are, as could be expected, the sites located in the south of Europe: the site that is the **most impacted is the Tagus estuary**, with successive MSI observations moderately or highly affected by sun glint; then, the Razelm-Sinoe Lagoon, observed at a single position in the swath, and moderately affected by sun glint in summer; and the Venice lagoon, either observed at the left of the swath without sun glint (but with only a partial observation), or at the centre-right part of the swath, with moderate to high impact of the sun glint.

For these sites, a partial or degraded monitoring can be expected with MSI if the atmospheric correction algorithm does not correct for sun glint contamination, with results depending on the seasons, and on the local sun glint intensity.

# 5  Visual inspection and decorrelation analysis

## 5.1  Method

**Sample OLCI and MSI products** were selected over the case study areas, and processed with each atmospheric correction algorithm. The top of atmosphere signal was first corrected for gaseous absorption and Rayleigh scattering to produce $\rho_{rc}(\lambda)$, and then decomposed by the atmospheric correction into two components: the water reflectance $\rho_w(\lambda)$, and the
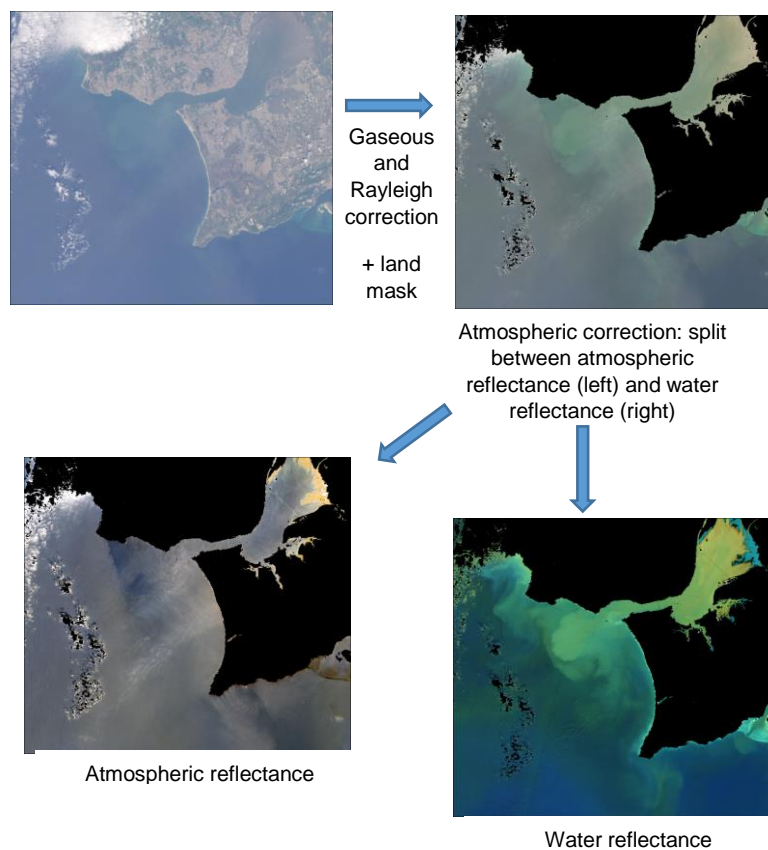
atmospheric path reflectance $\rho_{atm}(\lambda)$. While neglecting the aerosol transmission, the Rayleigh transmission term $t_{ray}$ is applied to the water reflectance.

$$\rho_{rc}(\lambda) = \rho_{atm}(\lambda) + t_{ray}(\lambda)\rho_w(\lambda)$$

In this section, we visualize the terms $\rho_{atm}(\lambda)$ and $\rho_w(\lambda)$, which are produced by each atmospheric correction algorithm. The term $\rho_{atm}(\lambda)$ is calculated for each algorithm from its estimation of $\rho_w(\lambda)$, using the values of $\rho_{rc}(\lambda)$ and $t_{ray}(\lambda)$ calculated by Polymer, and considered algorithm-independent.

Ideally, the atmospheric and water components should be **perfectly decoupled**: the RGB visualization (using bands 665, 560 and 443nm respectively) of these terms allows to see whether there are remaining water patterns on the atmospheric component, and vice-versa. A black colour indicates invalid or negative values.

The objective of this qualitative visualization is to understand and illustrate the main features of each atmospheric correction, with possibilities of further analysis by plotting transects (not done here), or undertaking validation exercises (done in section 5).



Gaseous
and
Rayleigh
correction

+ land
mask

Atmospheric correction: split
between atmospheric
reflectance (left) and water
reflectance (right)

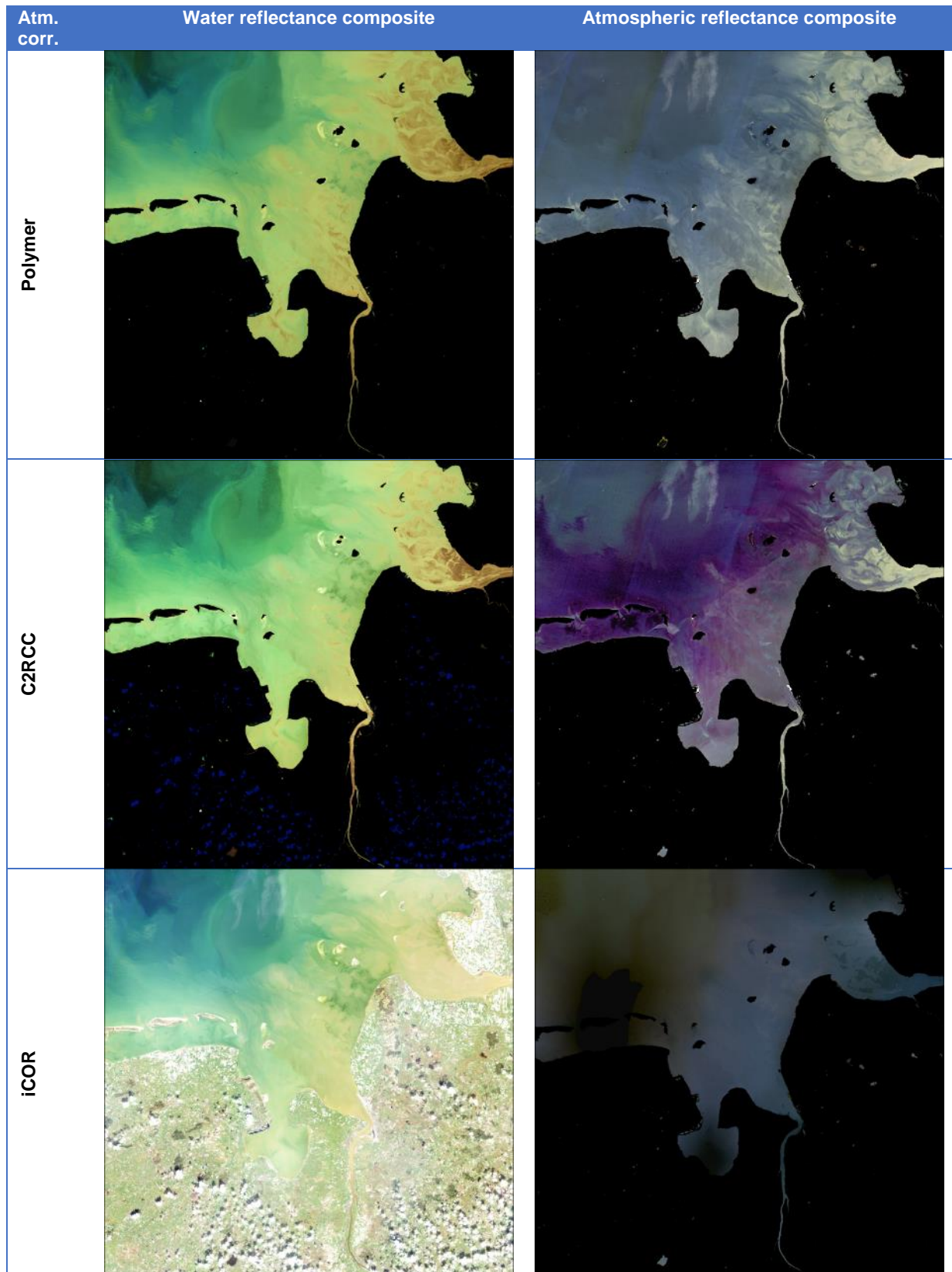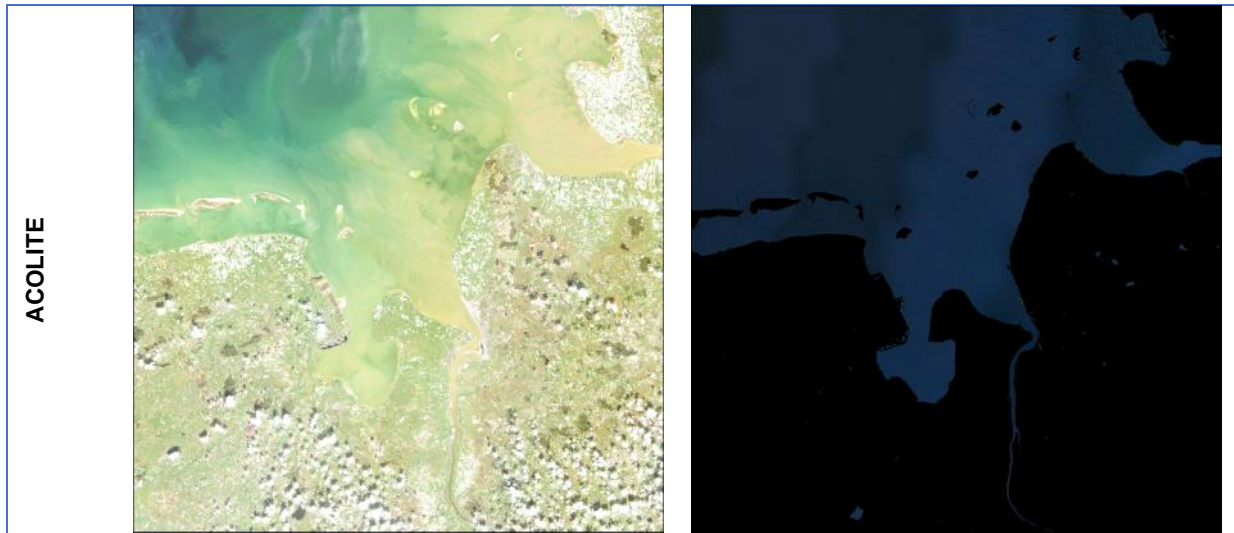Atmospheric reflectance

Water reflectance

*Figure 1: Illustration of the method to visualize the output of atmospheric correction algorithms, and in particular the quality of decoupling between the estimated atmospheric and water components of the signal.*

## 5.2 Results for MSI
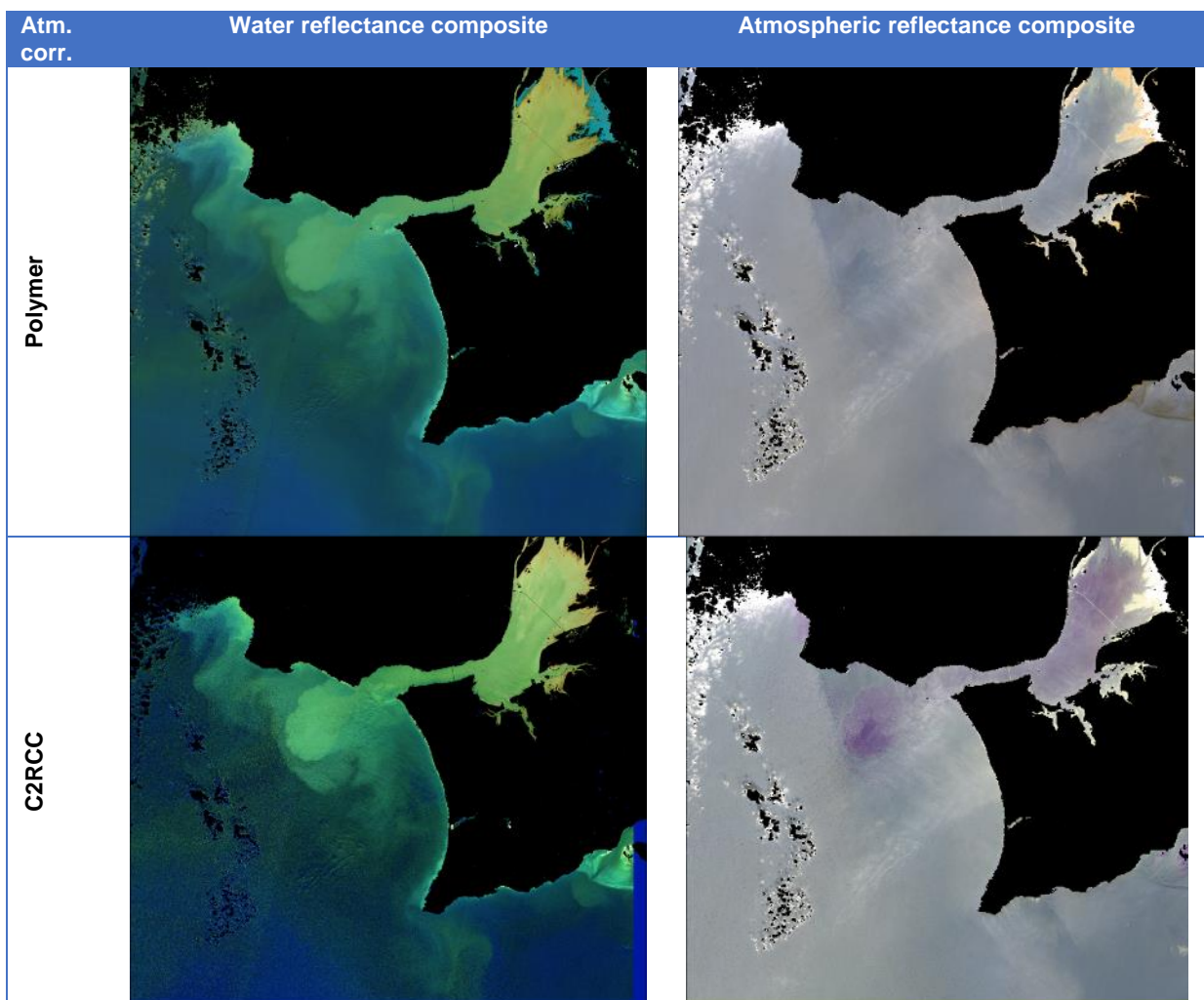
### 5.2.1 Elbe estuary/German Bight

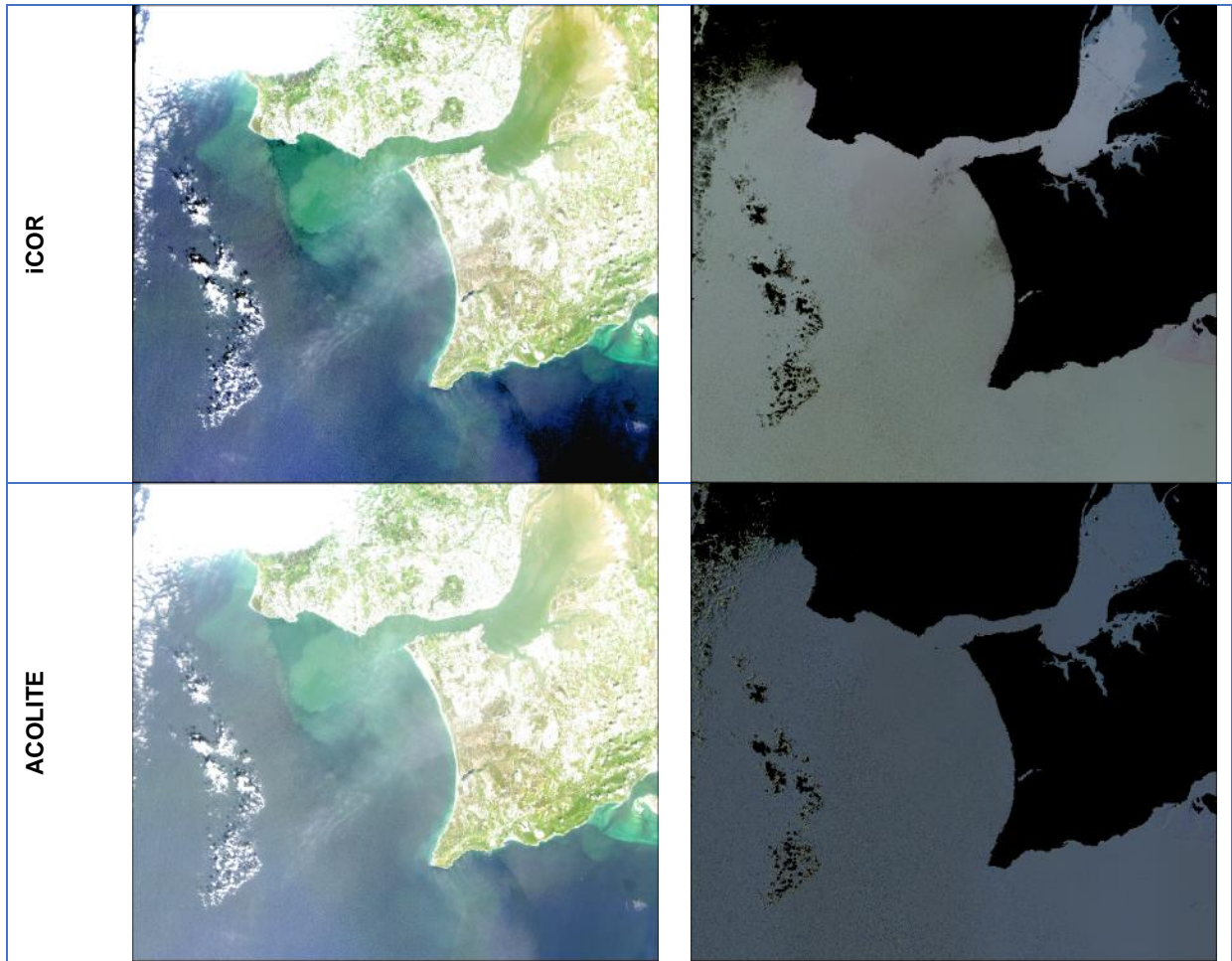S2A_MSIL1C_20200407T104021_N0209_R008_T32UME_20200407T110356

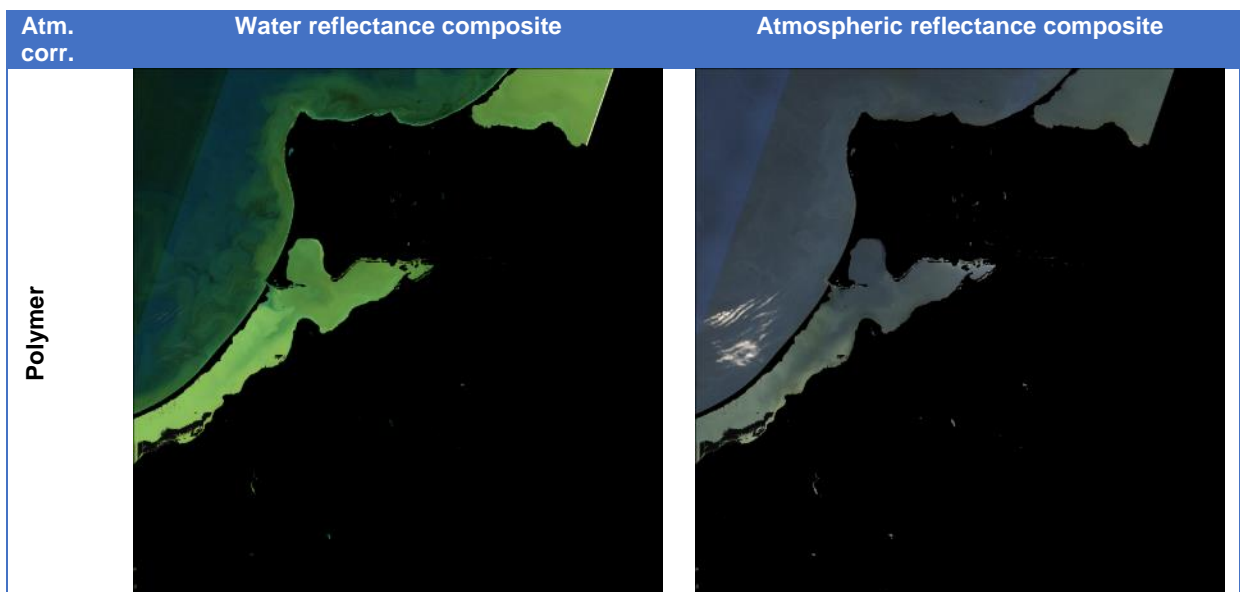| Atm. corr. | Water reflectance composite | Atmospheric reflectance composite |
|---|---|---|
| Polymer |  |  |
| C2RCC |  |  |
| iCOR |  |  |

| | |
|---|---|
| ACOLITE |  |

## 5.2.2 Tagus Estuary

S2B_MSIL1C_20200424T112109_N0209_R037_T29SMC_20200424T123554

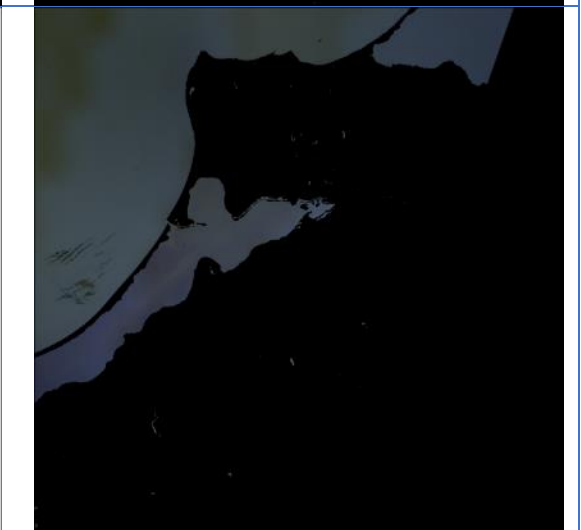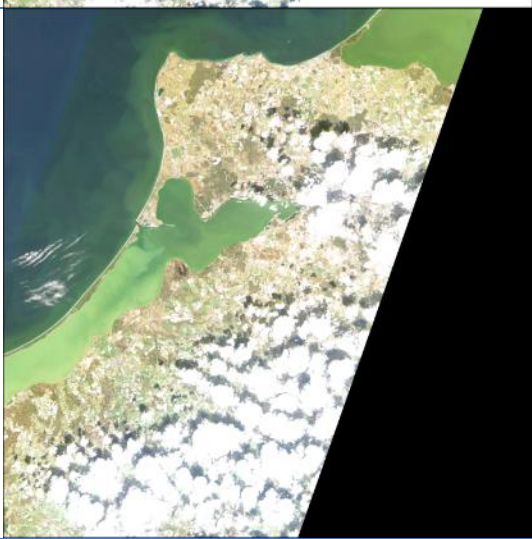| Atm. corr. | Water reflectance composite | Atmospheric reflectance composite |
|---|---|---|
| Polymer | | |
| C2RCC | | |

| | iCOR | |
| ACOLITE | | |
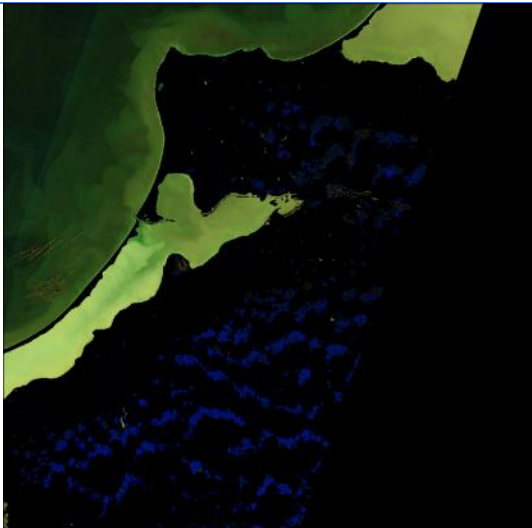
## 5.2.3 Curonian lagoon

S2B_MSIL1C_20200410T100029_N0209_R122_T34UDF_20200410T125625

| Atm. corr. | Water reflectance composite | Atmospheric reflectance composite |
| Polymer | | |

**C2RCC**

**iCOR**

**ACOLITE**

## 5.2.4 Tamar estuary / Plymouth Sound

S2A_MSIL1C_20200409T112111_N0209_R037_T30UVA_20200409T132421
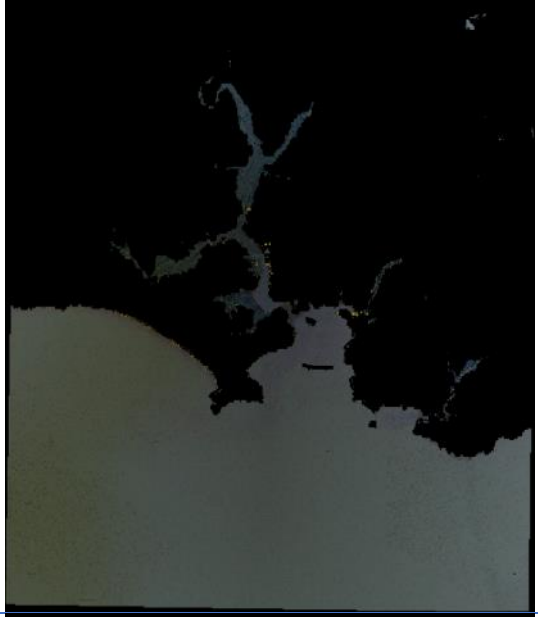
| Atm. corr. | Water reflectance composite | Atmospheric reflectance composite |
|---|---|---|
| Polymer |  |  |
| C2RCC |  |  |
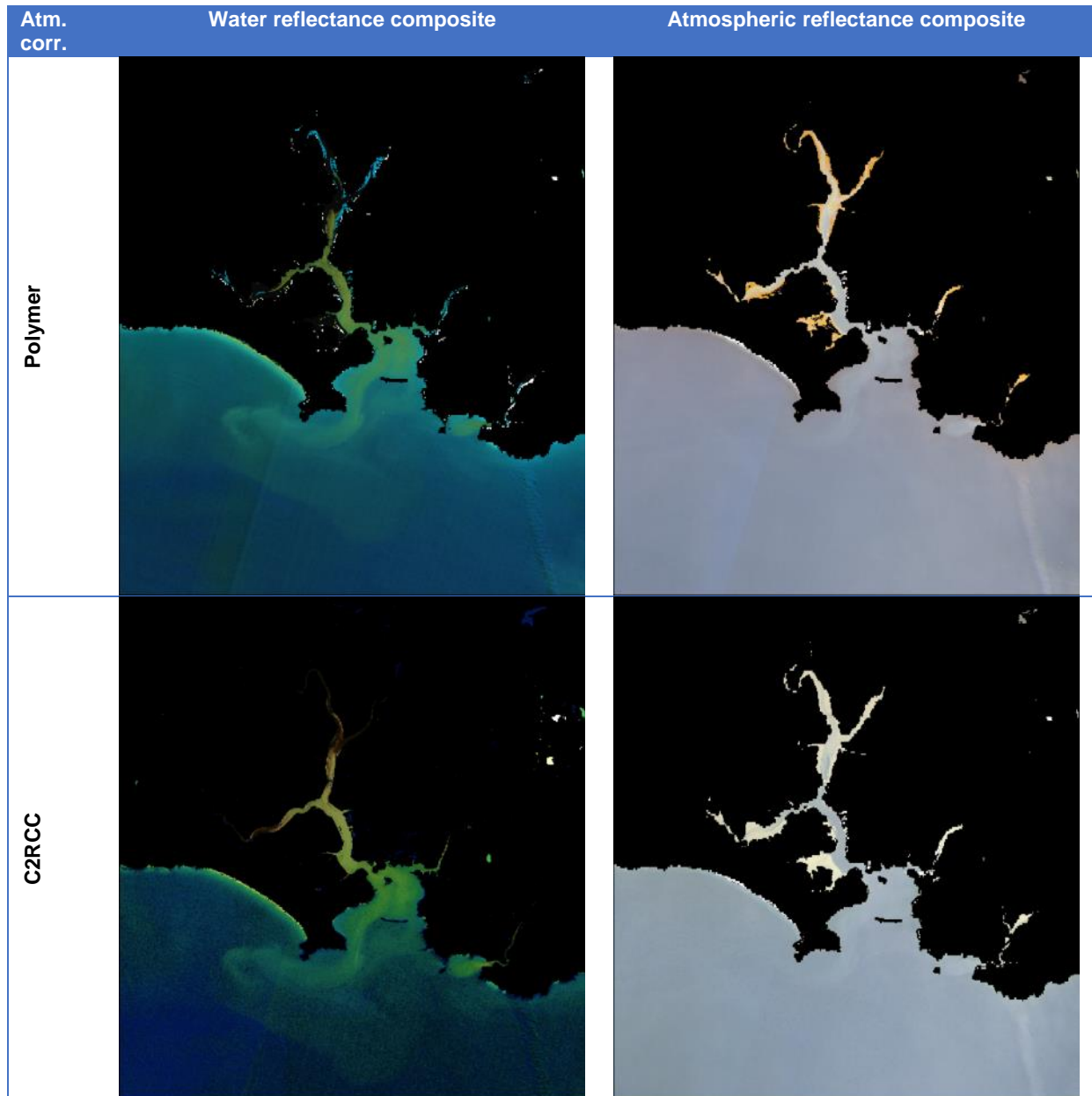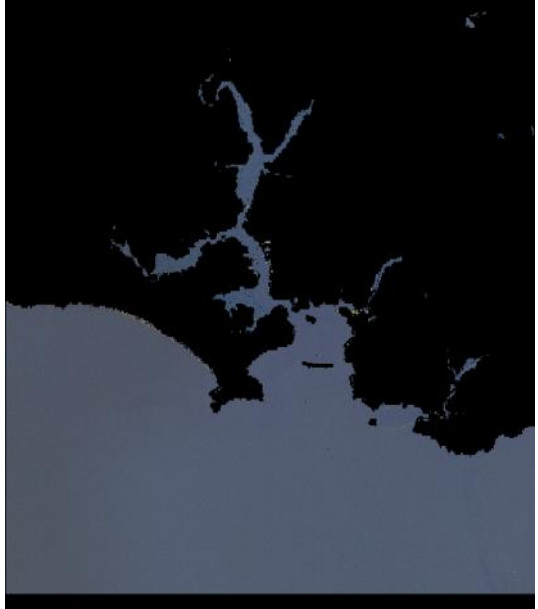
## 5.2.5  Razelm-Sinoe Lagoon System

S2A_MSIL1C_20200407T085551_N0209_R007_T35TPK_20200407T103455

| Atm. corr. | Water reflectance composite | Atmospheric reflectance composite |
|---|---|---|
| Polymer |  |  |
| C2RCC |  |  |
| iCOR |  |  |
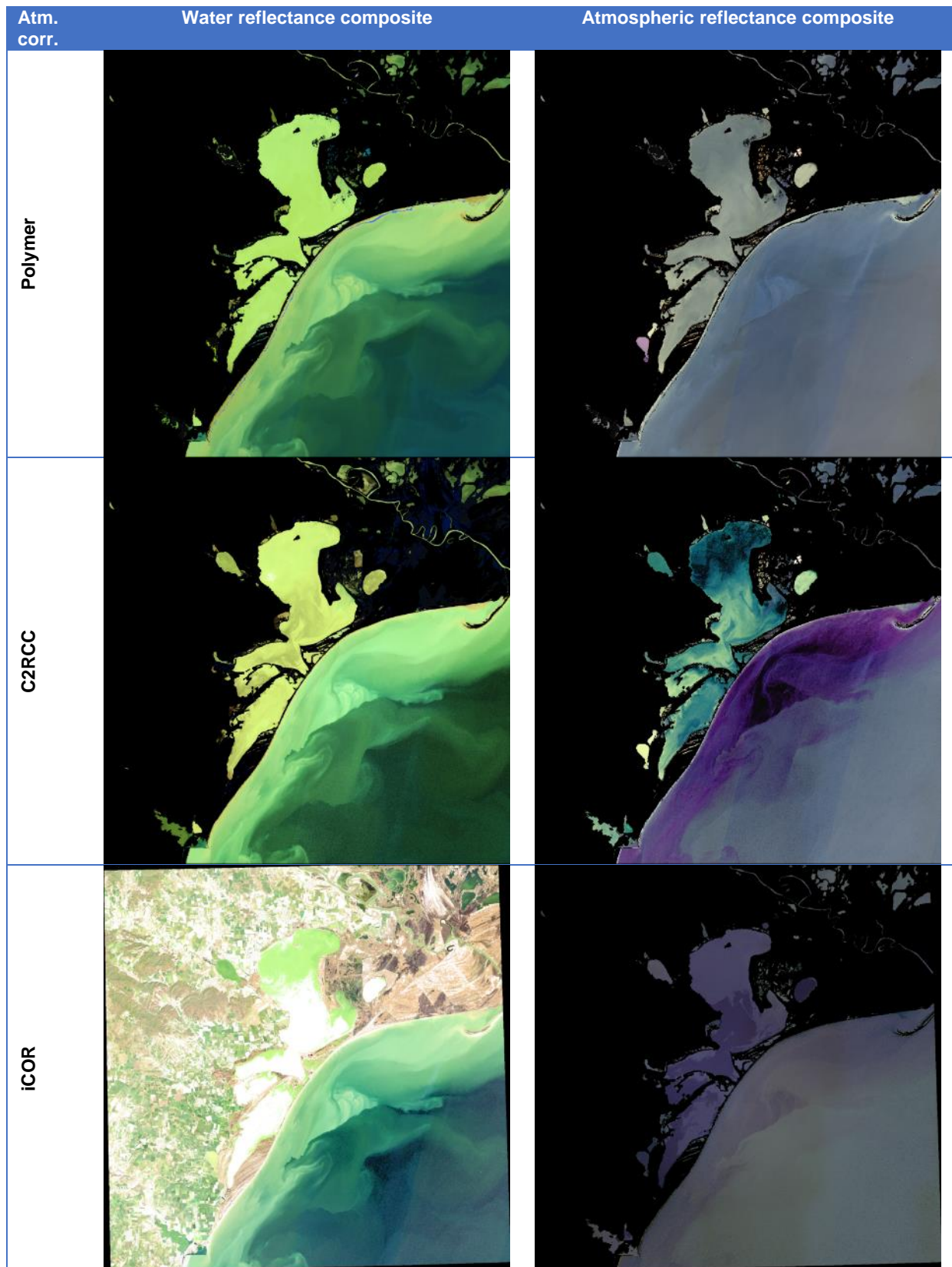
## 5.2.6 Venice lagoon

S2A_MSIL1C_20200408T101021_N0209_R022_T32TQR_20200408T153254

| Atm. corr. | Water reflectance composite | Atmospheric reflectance composite |
|---|---|---|
| Polymer | | |
| C2RCC | | |
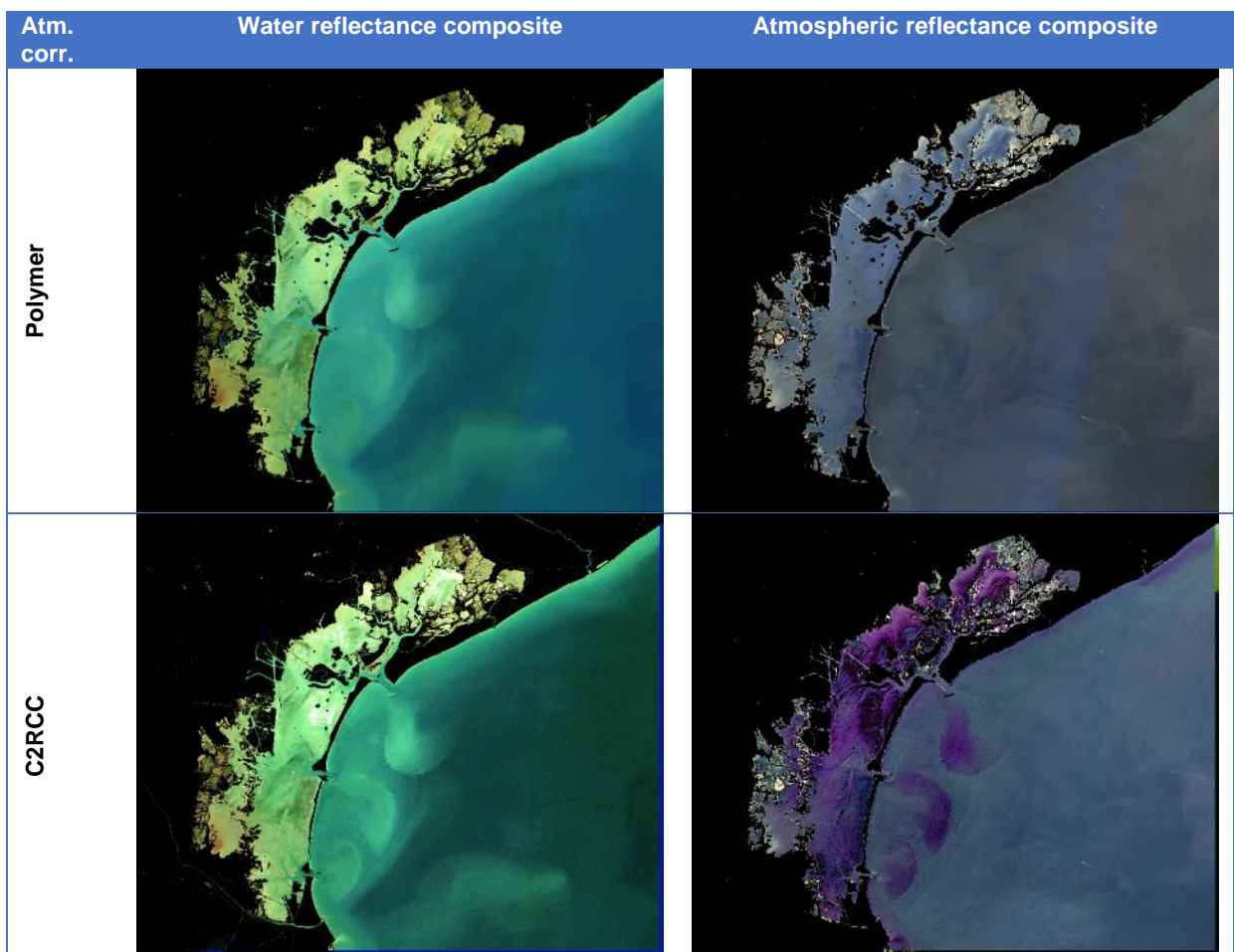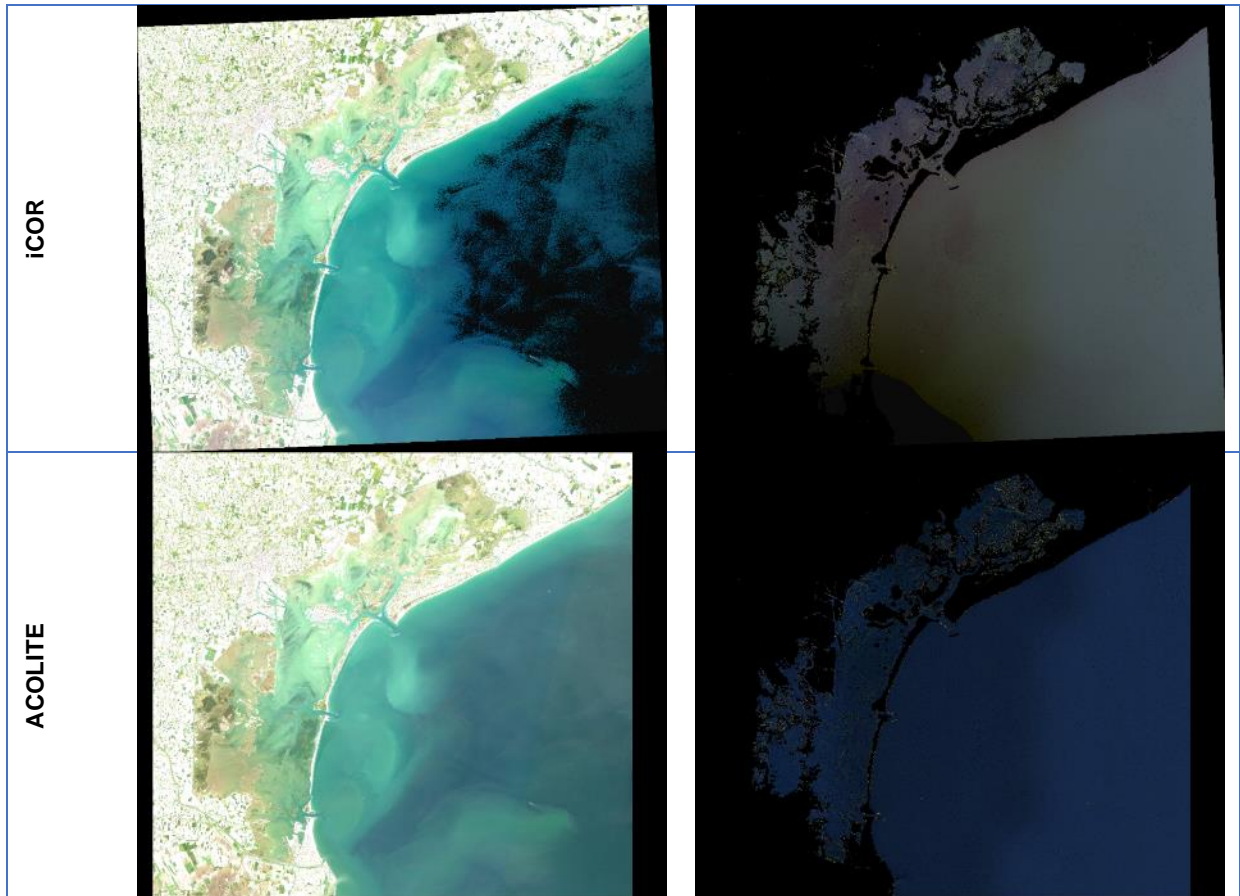
## 5.3 Results for OLCI

### 5.3.1 Elbe estuary/German Bight

S3A_OL_1_EFR____20200406T101735_20200406T102035_20200407T150905_0179_057
_008_1980_LN1_O_NT_002

| Atm. corr. | Water reflectance composite | Atmospheric reflectance composite |
| --- | --- | --- |
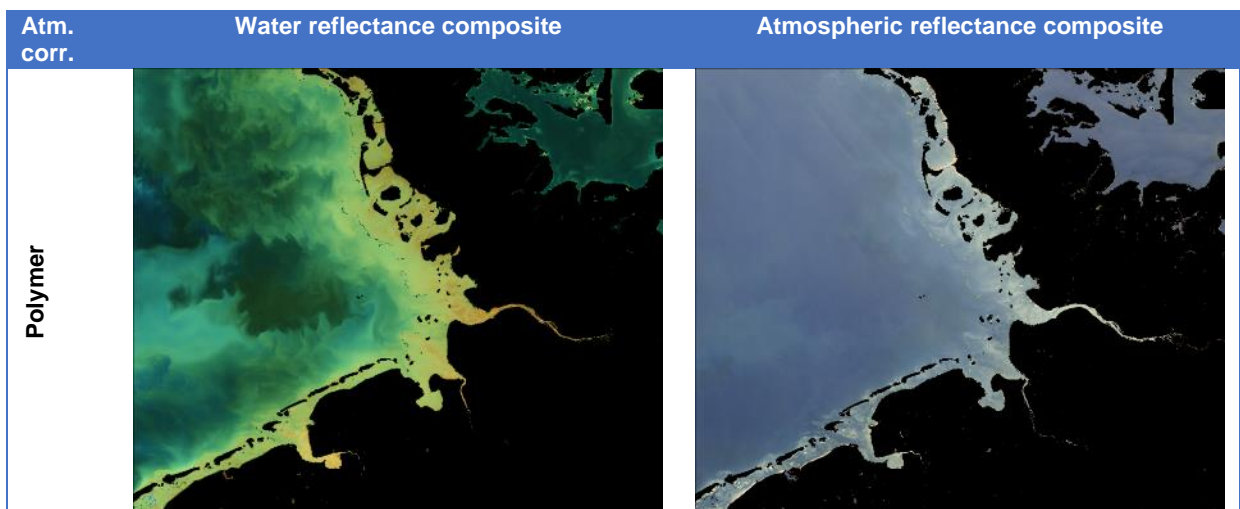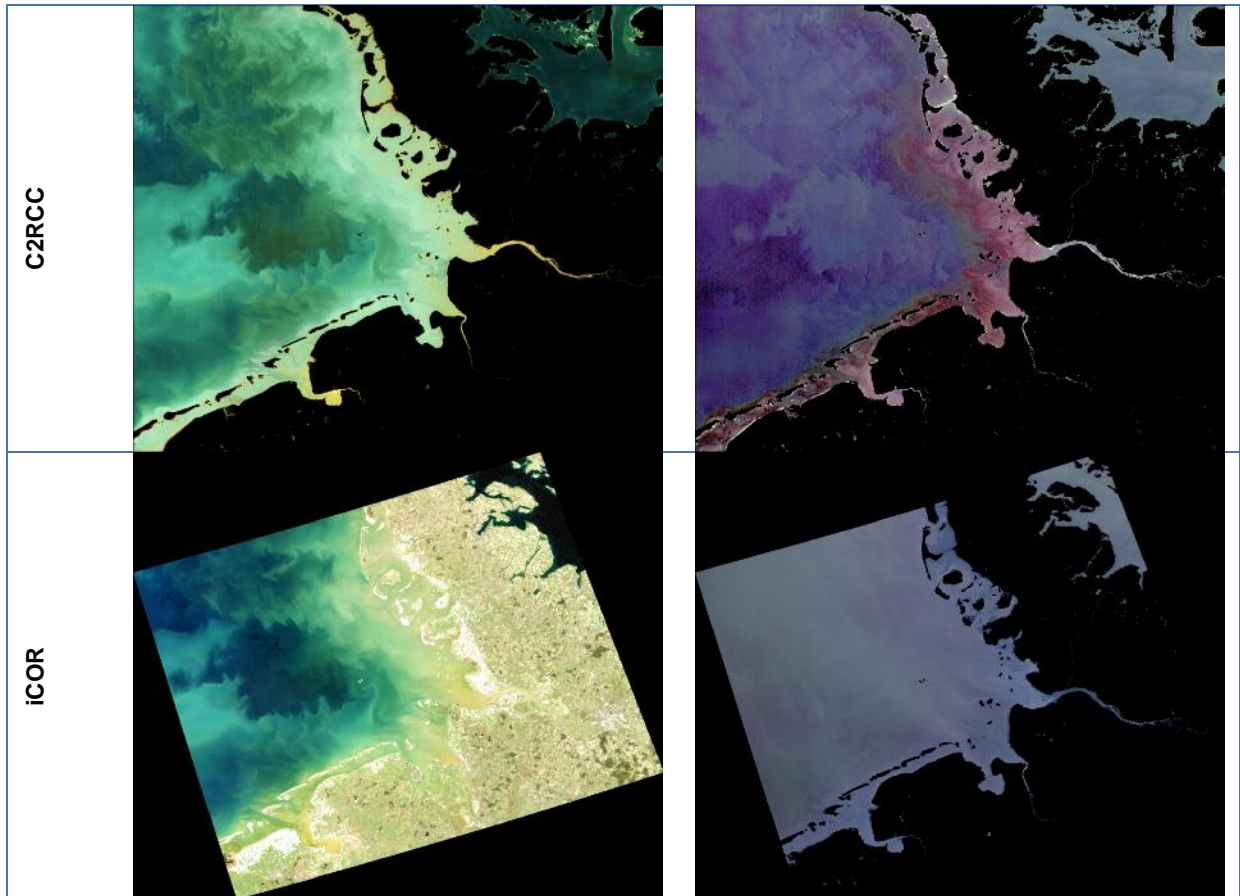
## 5.3.2 Tagus Estuary

S3A_OL_1_EFR____20200402T102719_20200402T103019_20200403T142621_0179_056
_336_2340_LN1_O_NT_002
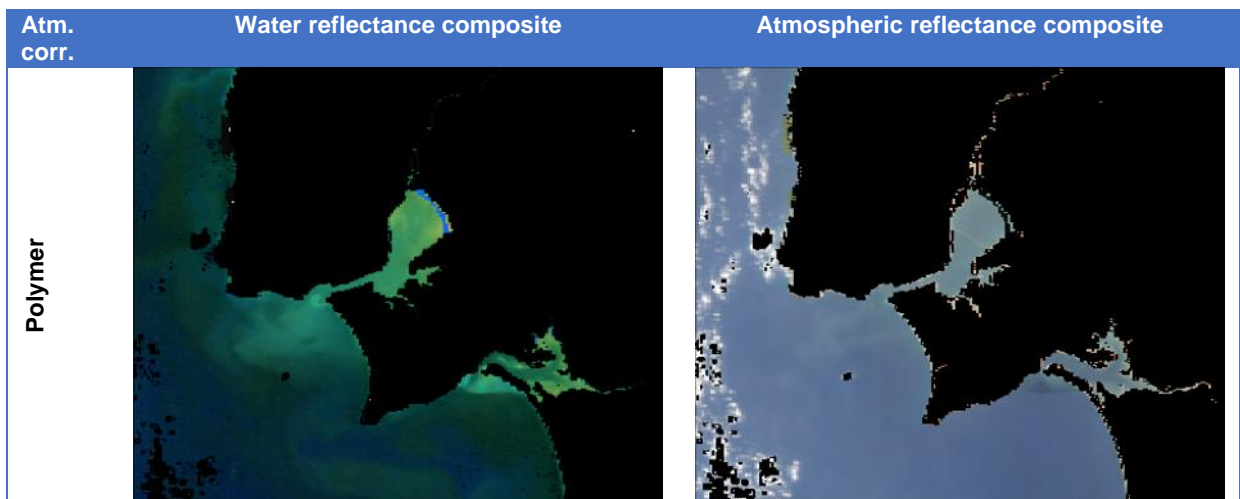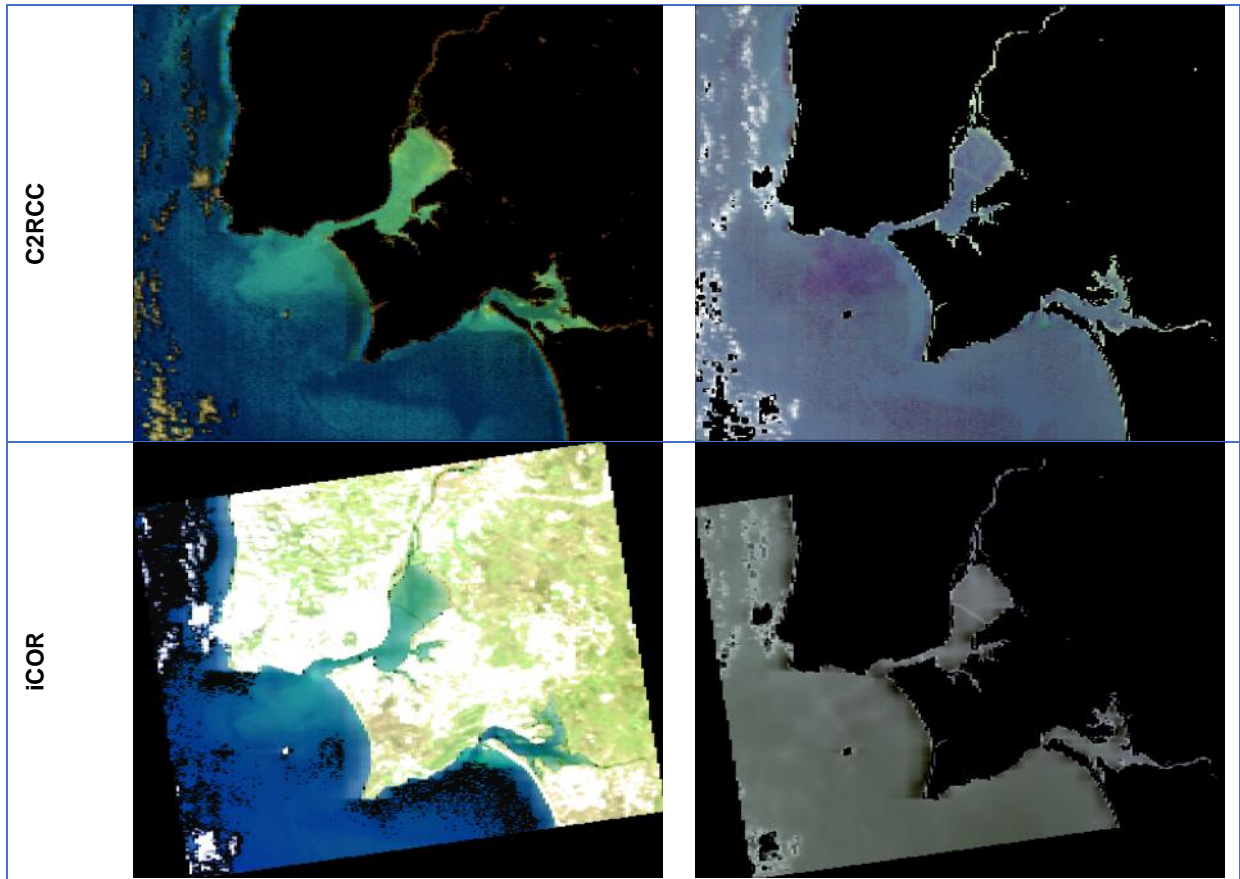
### 5.3.3 Curonian lagoon

S3B_OL_1_EFR____20200406T093801_20200406T094101_20200407T134625_0179_037
_250_1980_LN1_O_NT_002

| Atm. corr. | Water reflectance composite | Atmospheric reflectance composite |
|---|---|---|
| Polymer | | |

| Atm. corr. | Water reflectance composite | Atmospheric reflectance composite |
|---|---|---|
| C2RCC | | |
| iCOR | | |
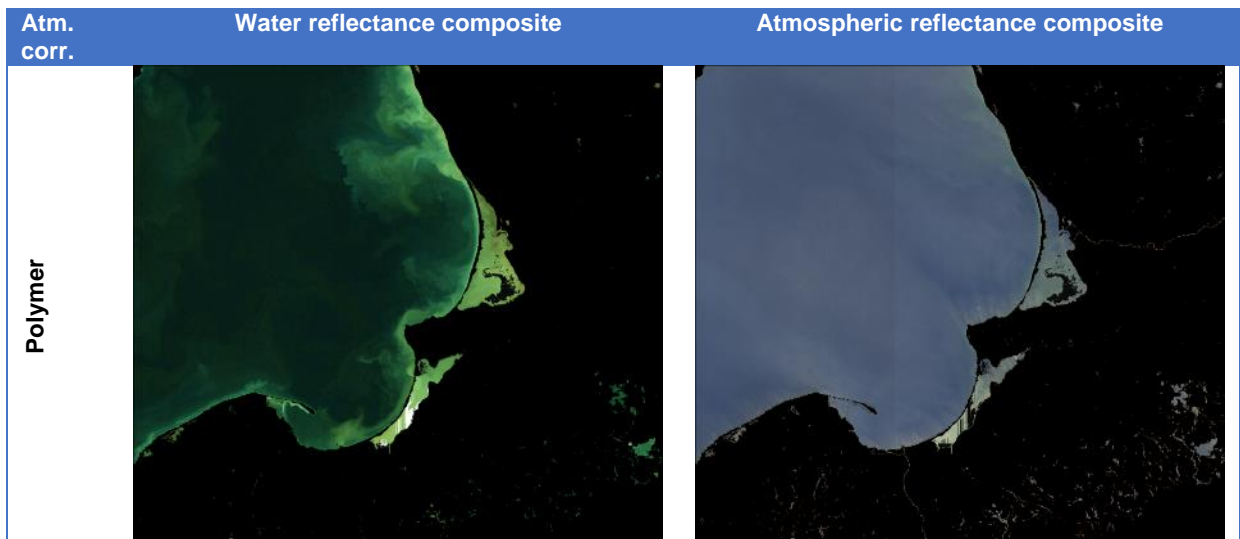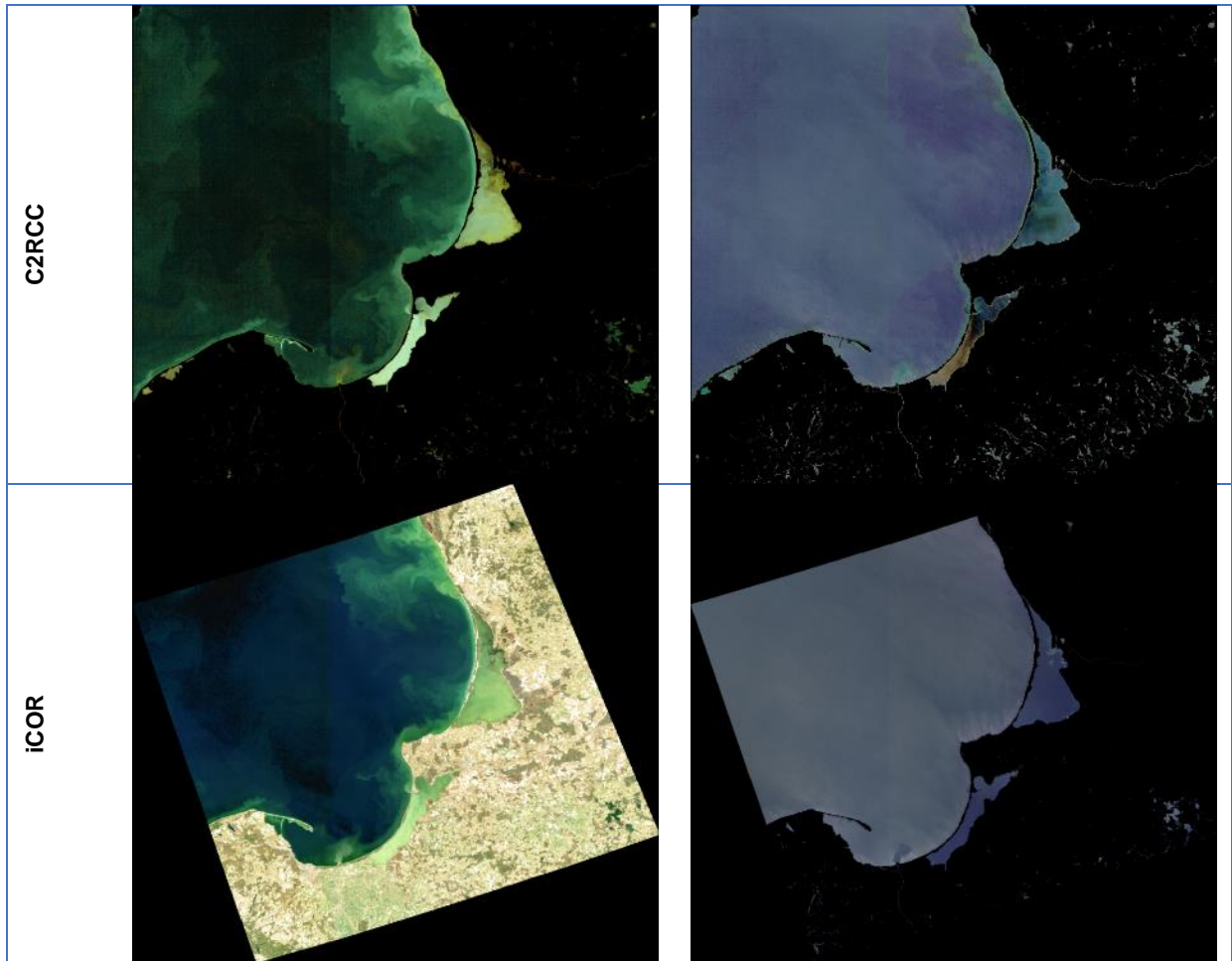
## 5.3.4 Tamar estuary / Plymouth Sound

S3A_OL_1_EFR____20200404T110957_20200404T111257_20200405T144706_0179_056 _365_1980_LN1_O_NT_002

| Atm. corr. | Water reflectance composite | Atmospheric reflectance composite |
|---|---|---|
| Polymer | | |
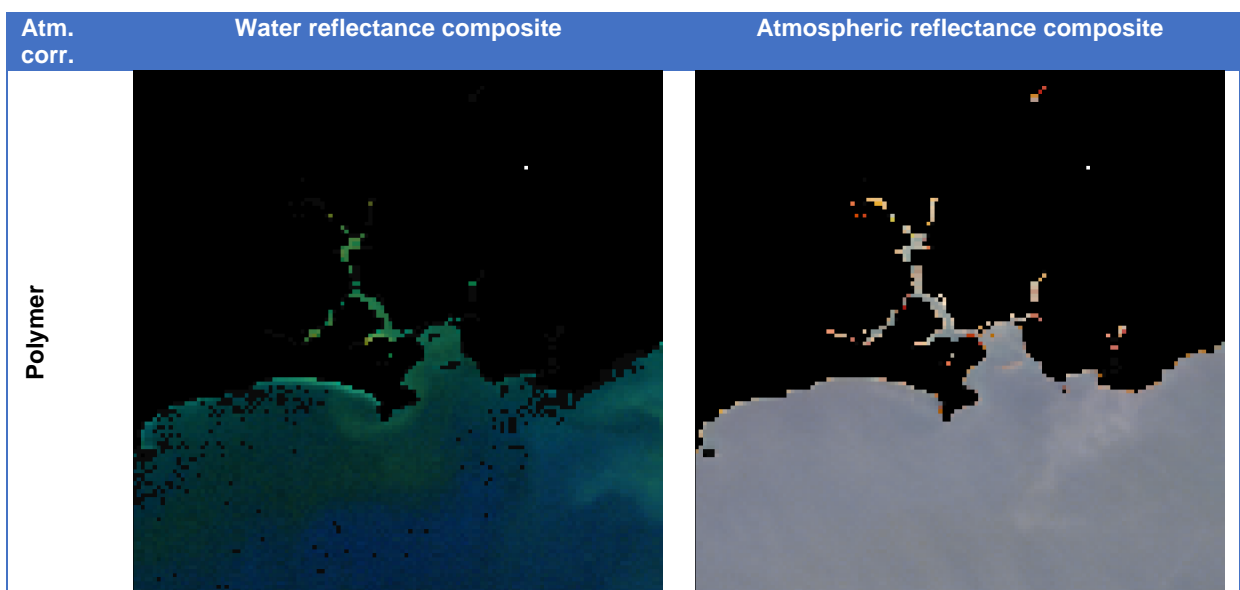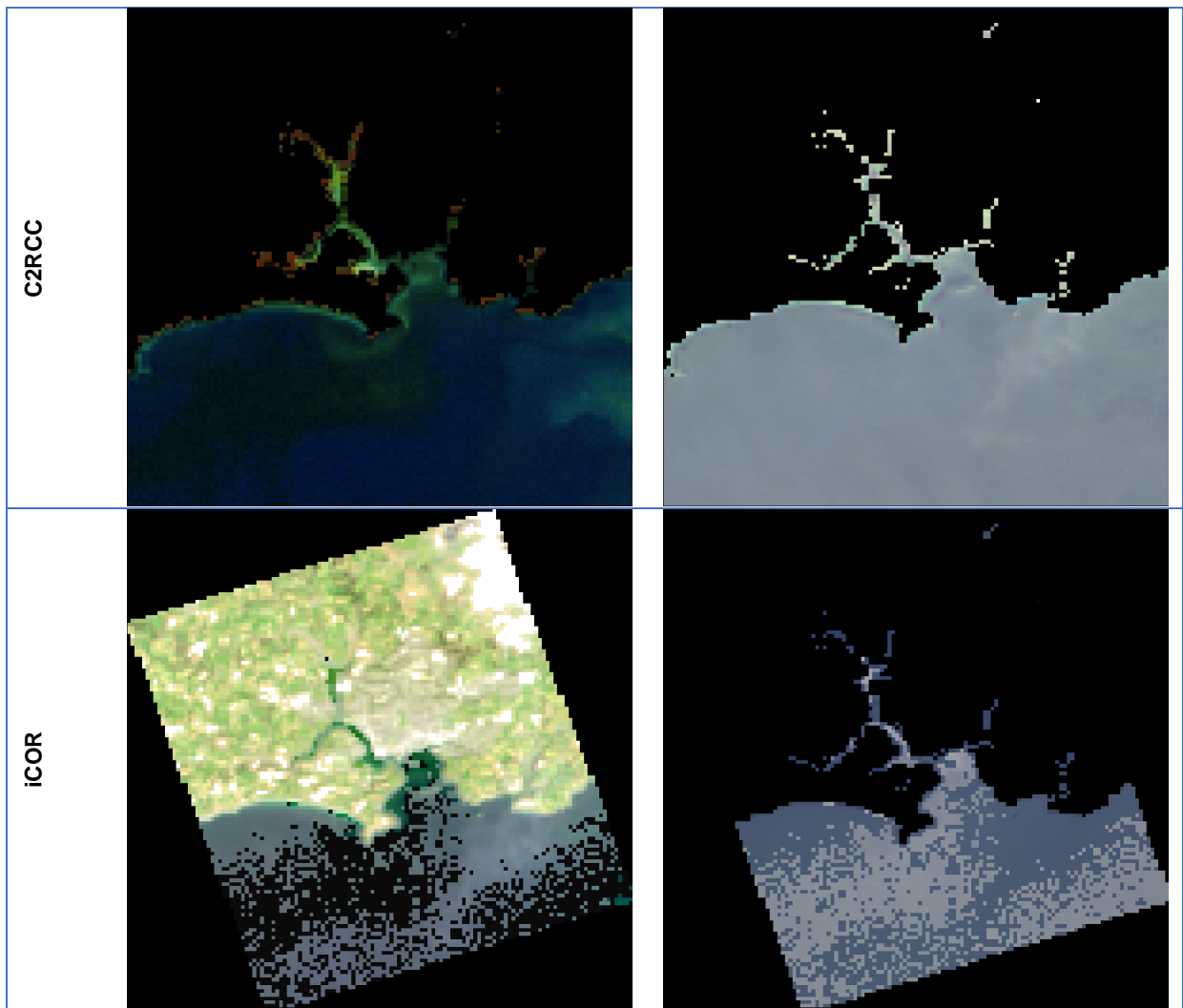
## 5.3.5 Razelm-Sinoe Lagoon System

S3A_OL_1_EFR____20200402T084320_20200402T084620_20200403T124743_0179_056
_335_2160_LN1_O_NT_002

| | Water reflectance composite | Atmospheric reflectance composite |
|---|---|---|
| **C2RCC** |  |  |
| **iCOR** |  |  |
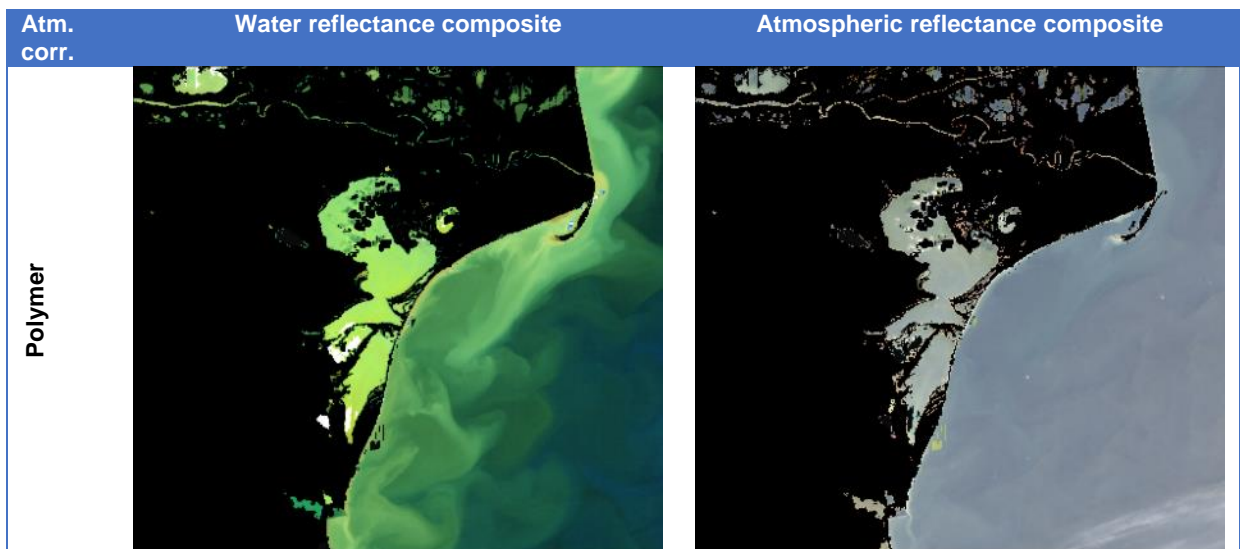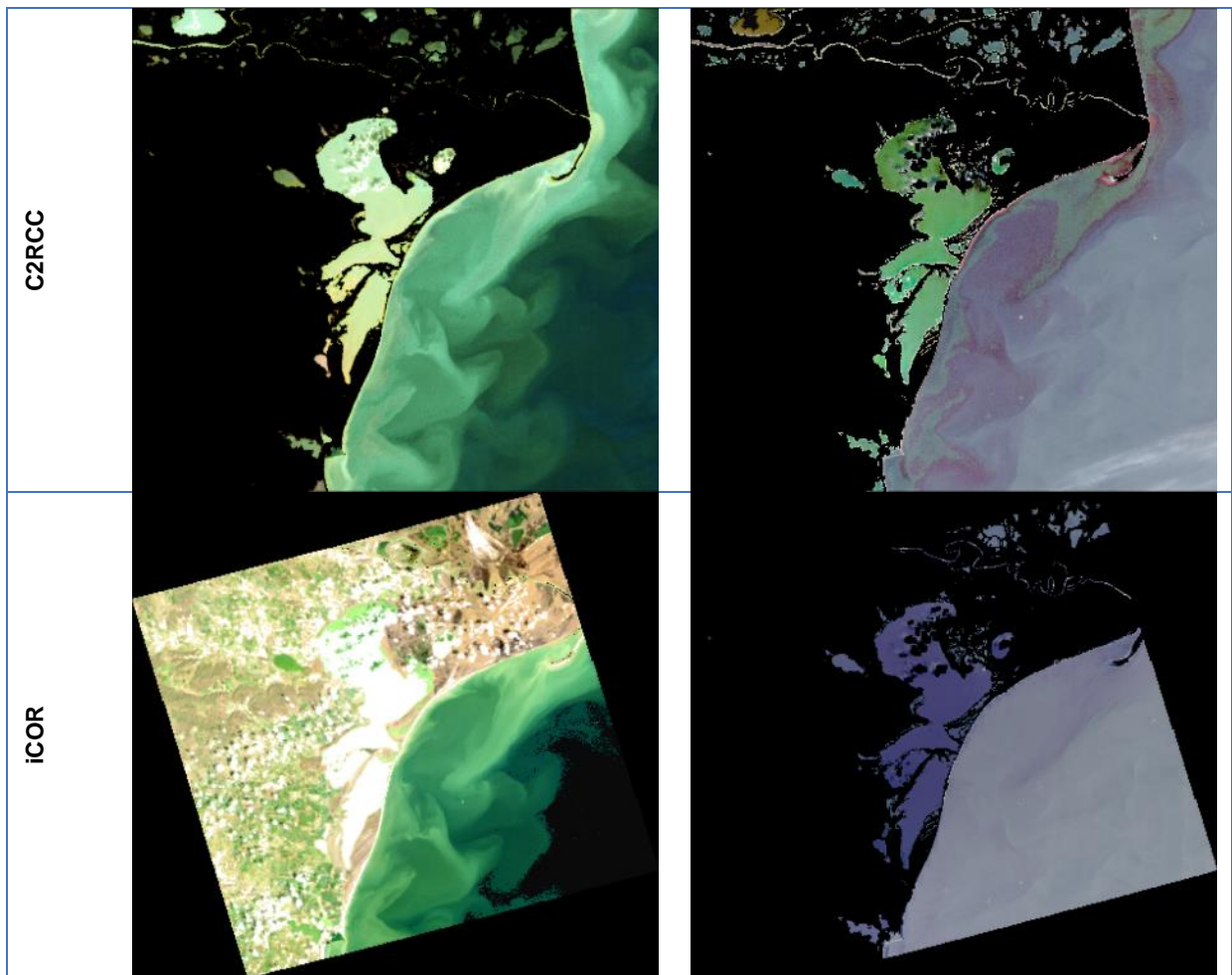
### 5.3.6 Venice lagoon

S3A_OL_1_EFR____20170420T093144_20170420T093444_20180417T025441_0179_016
_364_2160_LR2_R_NT_002

| Atm. corr. | Water reflectance composite | Atmospheric reflectance composite |
|---|---|---|
| **Polymer** |  |  |
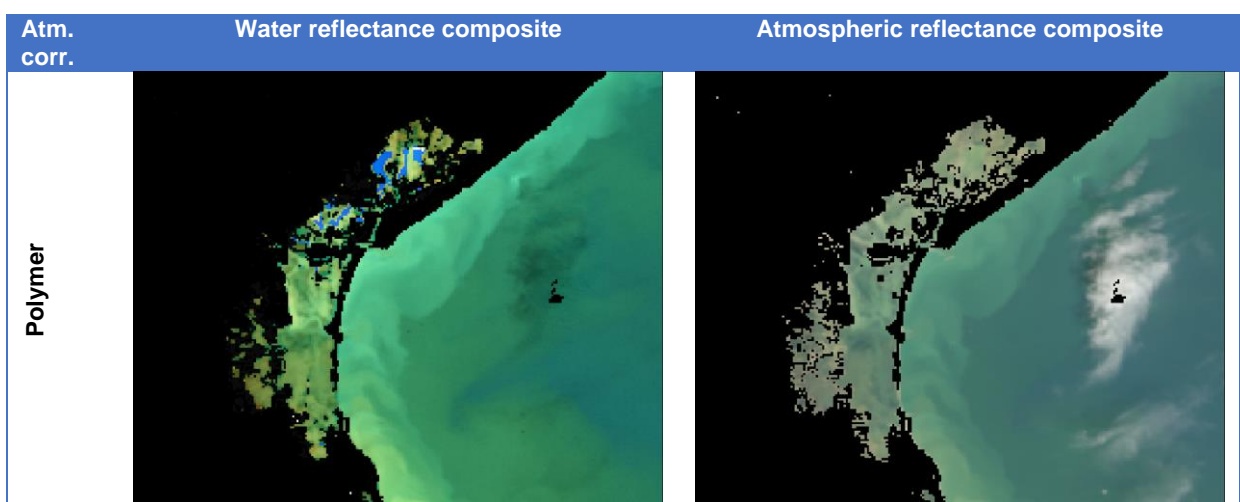
## 5.4  Discussion

Most of the scenes selected here are relatively clear and cloud-free, but some scenes contain clouds (5.2.3, 5.3.2, 5.3.6) or moderate sun glint (5.2.2). We can immediately observe that the **contamination by thin clouds or glint is well corrected by Polymer and C2RCC**, but not by **ACOLITE and iCOR**, which, by **assuming homogeneous atmospheric conditions across the image** (which can be visualized on the atmospheric reflectance composites), affect all small-scale atmospheric perturbations to the water component. See, for example, how the group of clouds at the west of the Vistula lagoon (5.2.3) is almost entirely affected to the atmosphere for Polymer and C2RCC, and entirely affected to the water for iCOR and ACOLITE.

We notice also that iCOR frequently retrieves negative reflectances, which appear in black on the plots. ACOLITE images of water reflectance appear brighter than the others (with darker images of atmospheric component); this positive bias will be confirmed by the validation exercise.

By construction, the determination of the atmospheric components in iCOR and ACOLITE is **independent of the water signal** (in ACOLITE, by considering 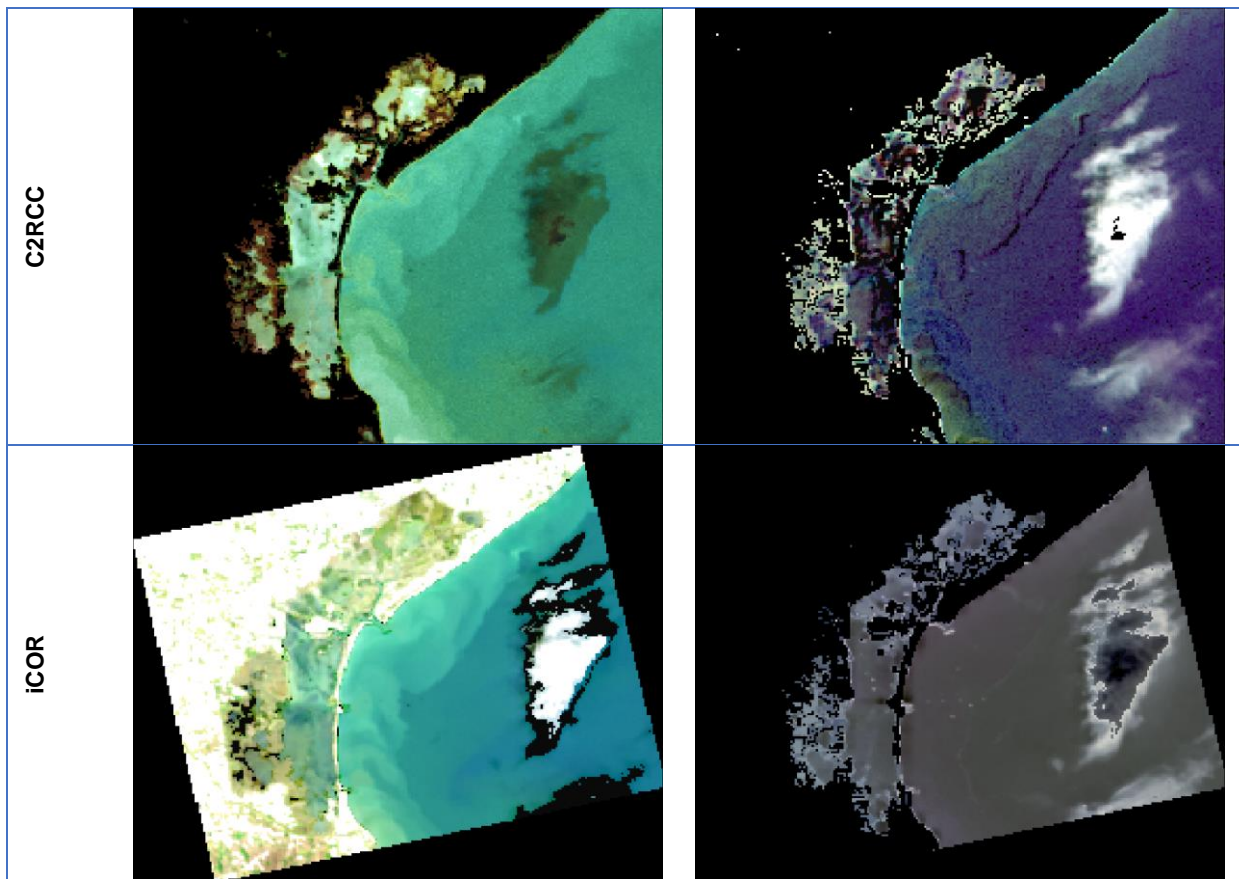SWIR bands, and in iCOR by considering land pixels), and, therefore, their atmospheric components do not show patterns related to the water signal. This is not true for Polymer and C2RCC which work pixel by pixel and rely on spectral bands that are affected by both the atmospheric and water signals. Polymer and C2RCC, therefore, show some **residuals of water patterns** on the atmospheric components:

- Polymer tends to overestimate the atmospheric component near coasts or in turbid areas, and, therefore, underestimates the water reflectance. See for example how the atmospheric component increases in brightness near the coast in the Elbe estuary/German bight (5.2.1, 5.3.1); however, this imperfect decoupling may also be due to the bathymetry effect (bottom visibility) or presence of unmasked emerged land (tidal zone). This effect will be studied further in WP5, in view of identifying which areas are affected by emerged land or bathymetry effect. Some impact of the water patterns is also visible in the Vistula lagoon (5.2.3), or as a different colour of the atmosphere between the Razelm-Sinoe lagoon and the nearby sea (5.2.5).
- Polymer shows some unstable regions with OLCI, but not with MSI. See for example some artefacts in the Curonian and Vistula lagoon (5.3.3). Research is underway to try and mitigate this effect in Polymer.
- C2RCC has generally more residual water patterns of the atmospheric component than Polymer. A purple colour appears sometimes in the atmospheric component, indicating that the green band is underestimated in the atmosphere, and, therefore, overestimated in the water. This purple colour appears sometimes at large scale (5.2.1; 5.3.6), and sometimes is limited to relatively small-scale water patterns (5.2.6). In the Venice example for OLCI, the atmospheric component appears in purple for the whole gulf of Venice: this may indicate a positive bias in the green band, which will be confirmed in the validation exercise for this site.

# 6 Validation using in-situ data

## 6.1 Method

This section presents the results of the validation of the four considered atmospheric correction algorithms, against **in-situ data from the AERONET-OC** measurements of the **Venice** site (Acqua Alta Oceanographic tower). Four sensors are considered here: MSI-A, MSI-B, OLCI-A and OLCI-B. The 'A' and 'B' versions of both MSI and OLCI are validated simultaneously, and the statistics are provided for respectively both OLCI-A and OLCI-B, and MSI-A and MSI-B, in order to provide a manageable number of results.

The MSI results are provided here at a 60m spatial resolution – all algorithms are capable of providing the outputs at 60m for all spectral bands. This spatial resolution is chosen over the 10 or 20m resolution because a high resolution is not required over the AERONET-OC Venice site, but higher spatial resolutions may be used with further, more appropriate in-situ data from the CERTO project.

*Comment: with iCOR, atmospheric correction at 10m of spatial resolution is only possible at the native MSI bands at 10m. Furthermore, iCOR does not support partial scene processing, and requires, therefore, for each match-up to process the full MSI or OLCI products.*

Polymer and C2RCC provide normalized reflectances (equivalent to sun and sensor at nadir), which are considered here. ACOLITE and iCOR provide bidirectional reflectances without normalization to a nadir-nadir geometry. The measurements from AERONET-OC include a directional normalization using the f/Q correction [Morel & Gentili 1996].

Examples of timeseries of AERONET-OC and estimations from Polymer are provided on the following figure:
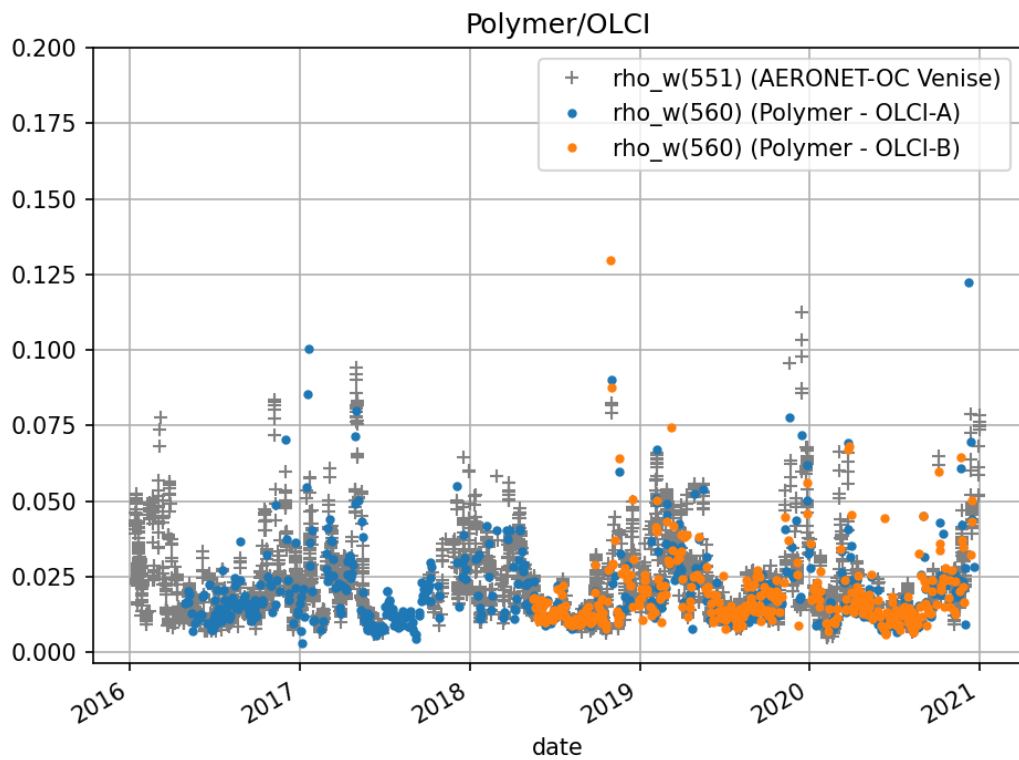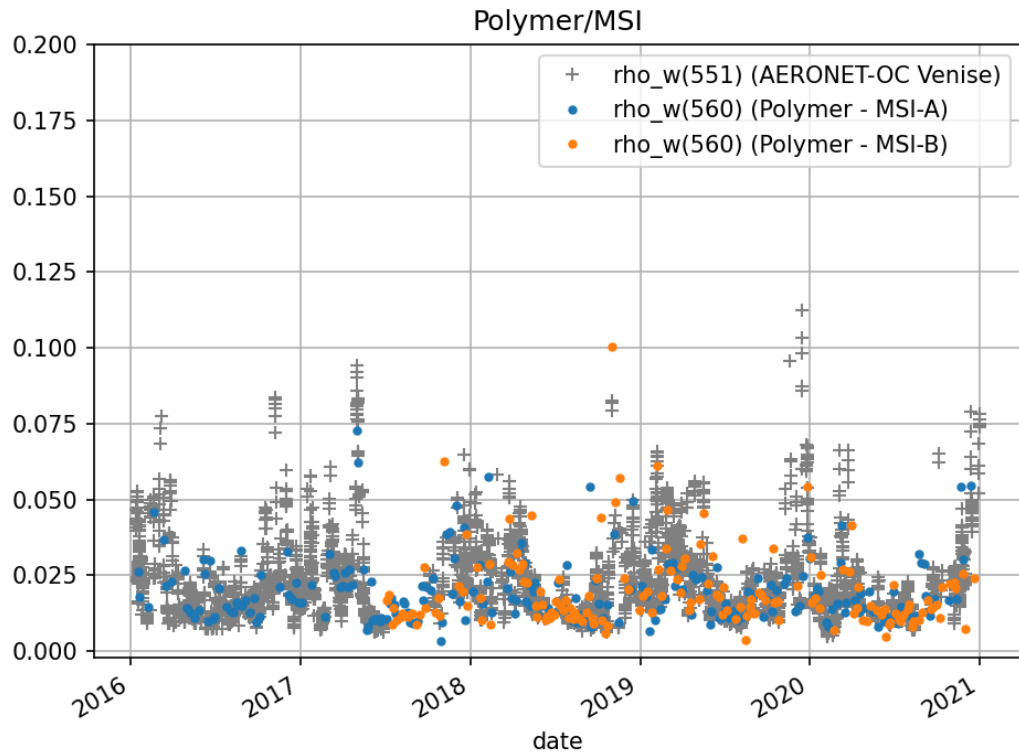
*Figure 6.1: timeseries of AERONET-OC Venice measurements and Polymer estimations of water reflectance at 560nm. Top: MSI (A and B), bottom: OLCI (A and B).*

**Flagging**

C2RCC and Polymer provide quality flags: the recommended flags are used to identify valid pixels.

- C2RCC's quality flags are: Cloud_risk, Rtosa_OOS, Rtosa_OOR, Rhow_OOS, Rhow_OOR
- Polymer's quality expression is: bitmask & 1023 != 0 (flags: land, cloud_base, L1_invalid, negative_bb, out_of_bounds, exception, thick_aerosol, high_air_mass)

iCOR and ACOLITE do not provide quality flags, except from the presence of NaN values. Furthermore, iCOR being scene-based fails over cloudy scenes and does not return any result. The MSI products cover a smaller region than OLCI products, therefore, fully cloudy situations are more frequent with MSI than OLCI, and iCOR fails more frequently with MSI. In our case, 389 out of 612 MSI products have been processed, and 1700 out of 1762 OLCI products.

iCOR and ACOLITE do not include a cloud mask. Therefore, Polymer's cloud mask (which is not strict, and leaves thin clouds) is applied to iCOR and ACOLITE results as a minimum.

The validation is performed at bands 412, 443, 490, 560 and 665nm for OLCI, and 443, 490, 560 and 665nm for MSI. These bands are chosen based on the availability of AERONET bands 412, 441, 488, 551 and 667nm (band shifting is not applied). On the results presented in next section, only the plots at 443, 560 and 665 nm are presented. For the other bands, the statistical values are given.

The "**individual best quality**" evaluation corresponds to using the filter previously described, to each algorithm individually. However, this case leaves many outliers for iCOR and ACOLITE, making the comparison difficult. Therefore, a second case is evaluated, "**common best quality**", where only the intersection of all valid pixels across 3 (OLCI) or 4 (MSI) algorithms are considered.


**Statistical values**

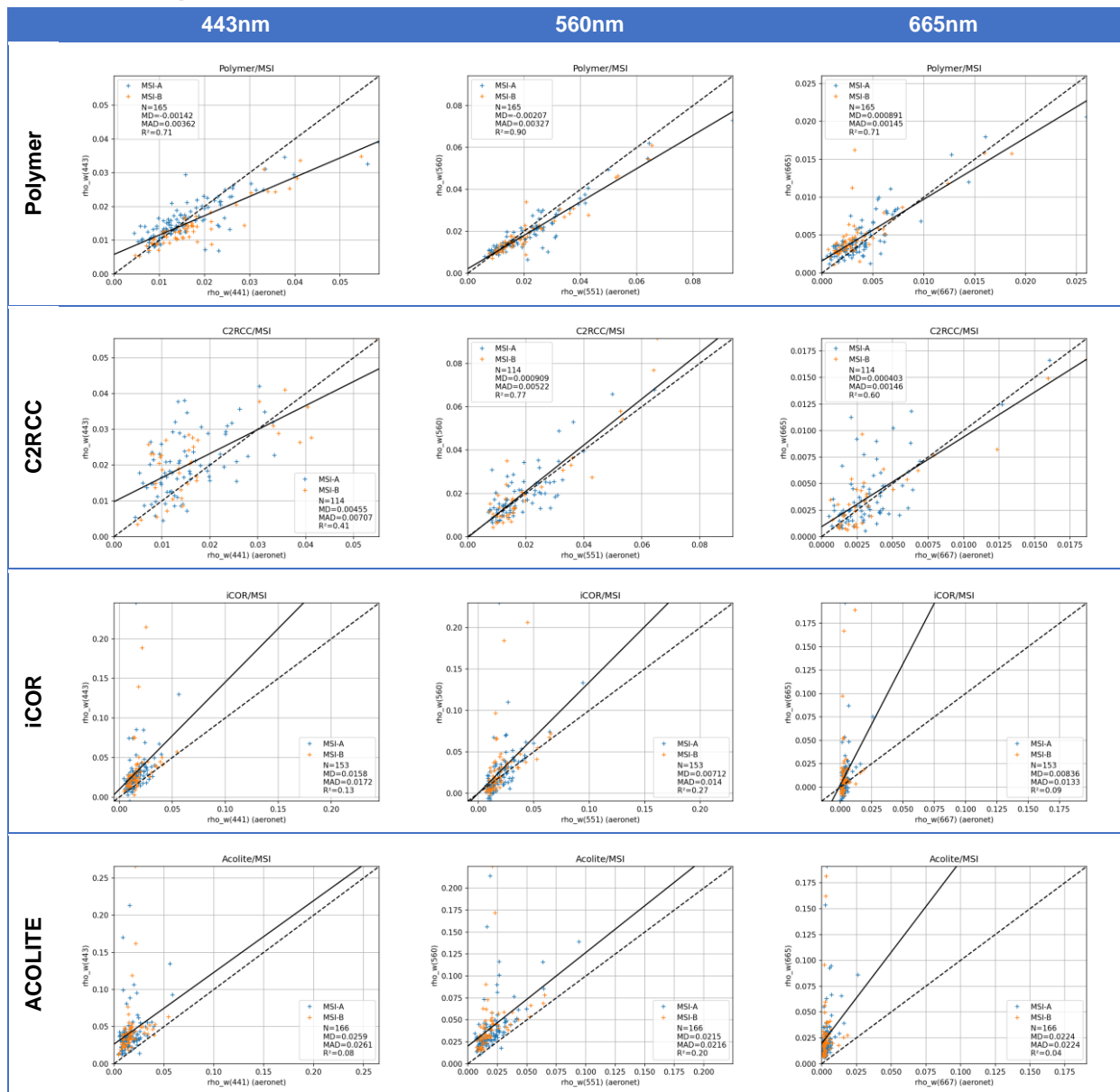The following statistical values are provided for evaluation of the matchups:

- Number of valid matchups
- Mean difference: $MD_\lambda = \frac{1}{n}\sum(\rho_w(\lambda_i)_{sat} - \rho_w(\lambda_i)_{insitu})$
- Mean absolute difference: $MAD_\lambda = \frac{1}{n}\sum |\rho_w(\lambda_i)_{sat} - \rho_w(\lambda_i)_{insitu}|$

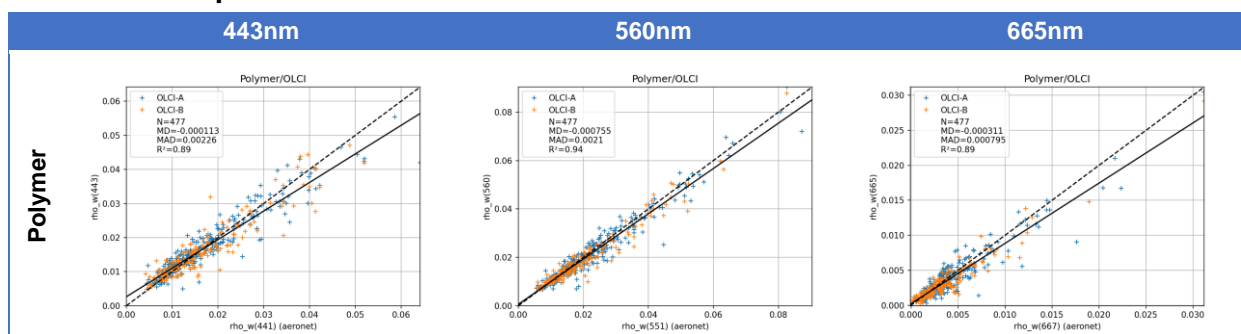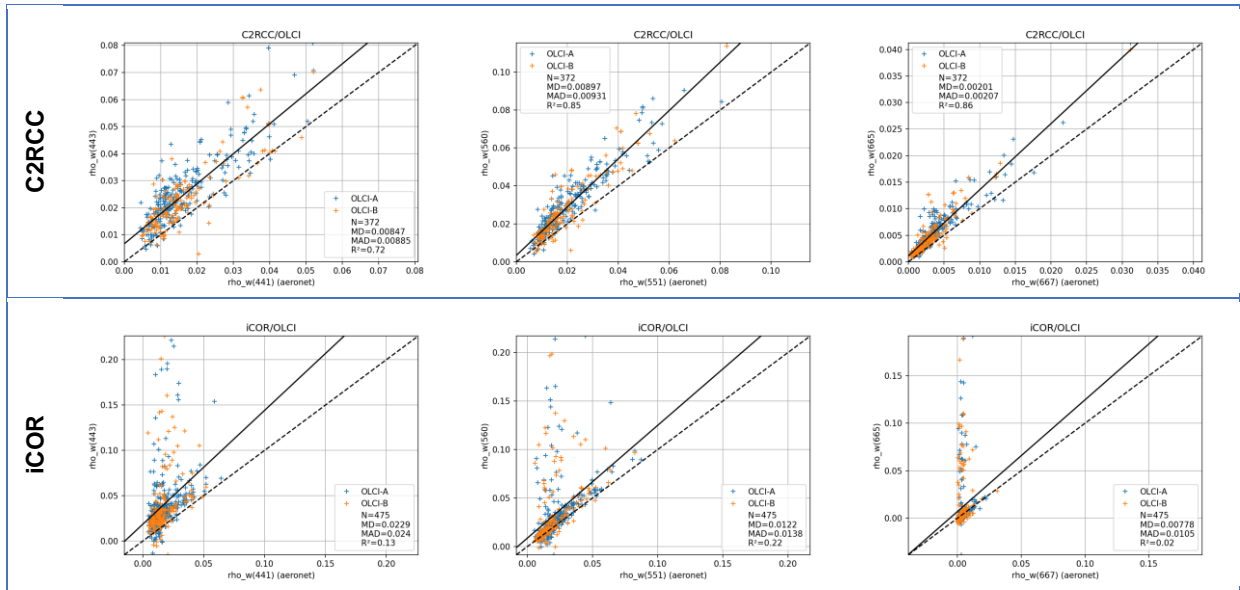## 6.2 Results

### 6.2.1 Individual best quality

#### 6.2.1.1 MSI plots



#### 6.2.1.2 OLCI plots

### 6.2.1.3 Statistics

| Algorithm | Sensor | N | Mean difference (MD) | | | | | Mean absolute difference (MAD) | | | | |
|---|---|---|---|---|---|---|---|---|---|---|---|---|
| | | | 412nm | 443nm | 490nm | 560nm | 665nm | 412nm | 443nm | 490nm | 560nm | 665nm |
| Polymer | OLCI | 477 | -0.000866 | -0.000113 | -0.00168 | -0.000755 | -0.000311 | 0.00326 | 0.00226 | 0.00249 | 0.0021 | 0.000795 |
| C2RCC | | 372 | 0.0052 | 0.00847 | 0.0119 | 0.00897 | 0.00201 | 0.00603 | 0.00885 | 0.0122 | 0.00931 | 0.00207 |
| iCOR | | 475 | 0.0286 | 0.0229 | 0.018 | 0.0122 | 0.00778 | 0.0298 | 0.024 | 0.0191 | 0.0138 | 0.0105 |
| Polymer | MSI | 165 | | -0.00142 | -0.00226 | -0.00207 | 0.000891 | | 0.00362 | 0.00451 | 0.00327 | 0.00145 |
| C2RCC | | 114 | | 0.00455 | 0.00406 | 0.000909 | 0.000403 | | 0.00707 | 0.00703 | 0.00522 | 0.00146 |
| iCOR | | 153 | | 0.0158 | 0.0115 | 0.00712 | 0.00836 | | 0.0172 | 0.0152 | 0.014 | 0.0133 |
| Acolite | | 166 | | 0.0259 | 0.0228 | 0.0215 | 0.0224 | | 0.0261 | 0.0231 | 0.0216 | 0.0224 |

*Figure 6.2: Statistical values associated with the validation of MSI and OLCI products over the AERONET-OC Venice site in the "individual best quality" dataset.*
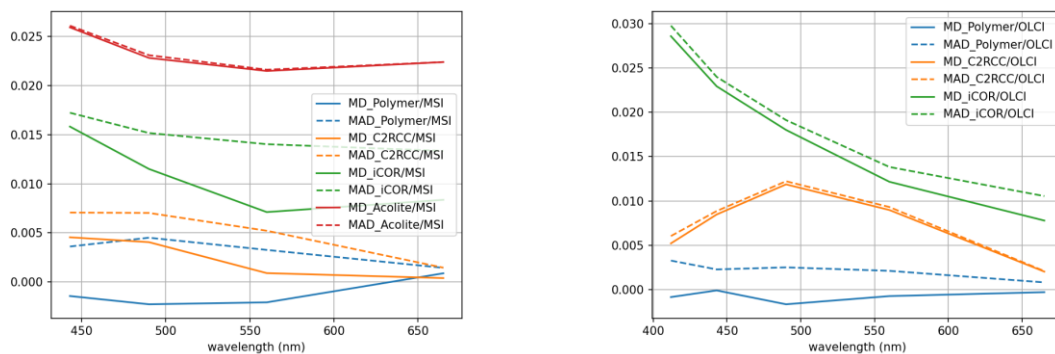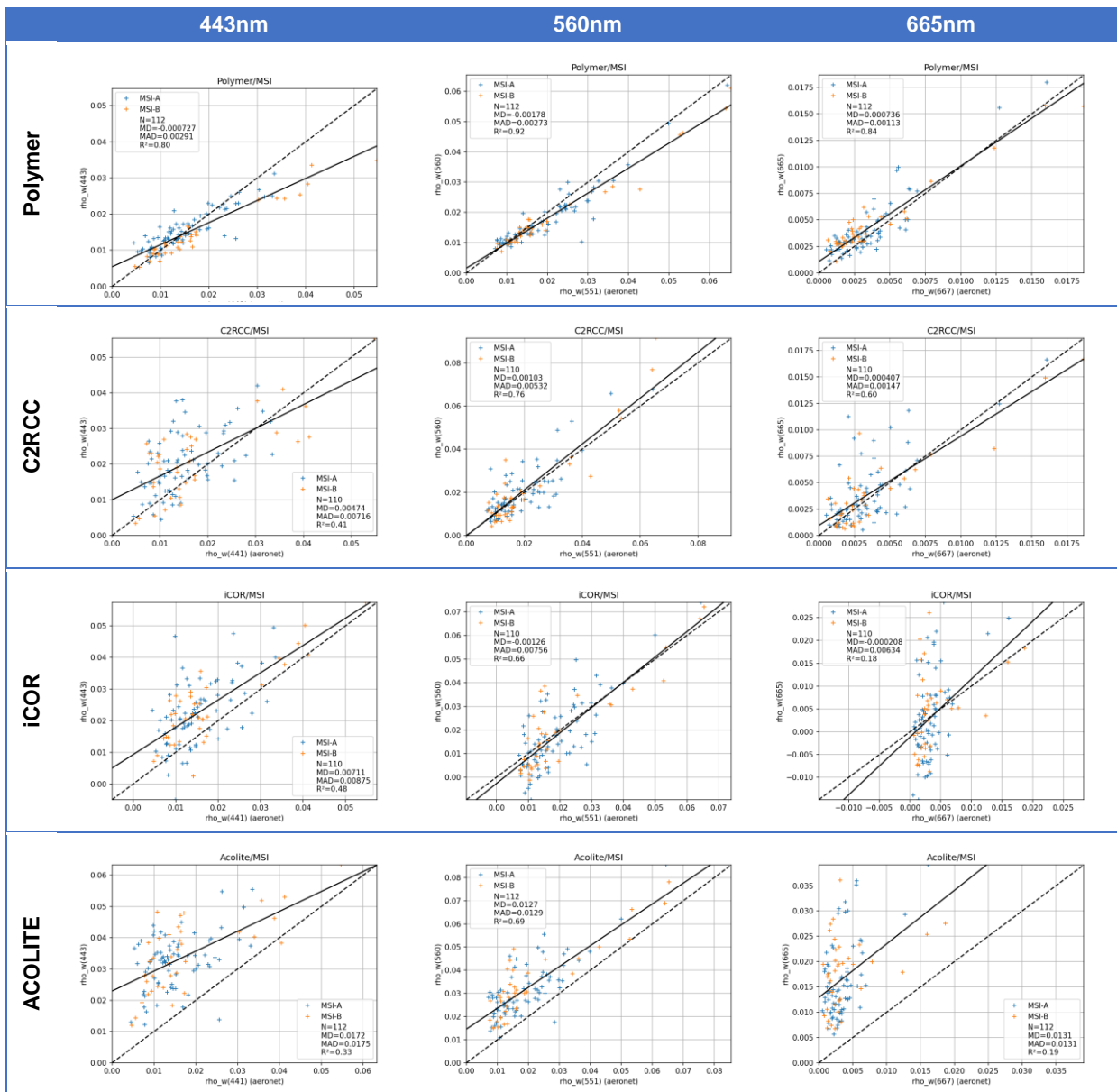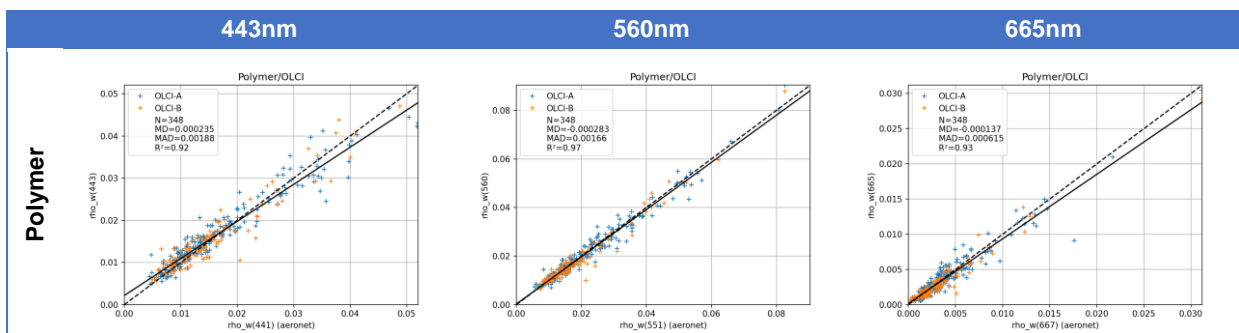


*Figure 6.3: MD and MAD plotted as a function of the wavelength, for each algorithm applied to MSI (left) and OLCI (right) – individual best quality*
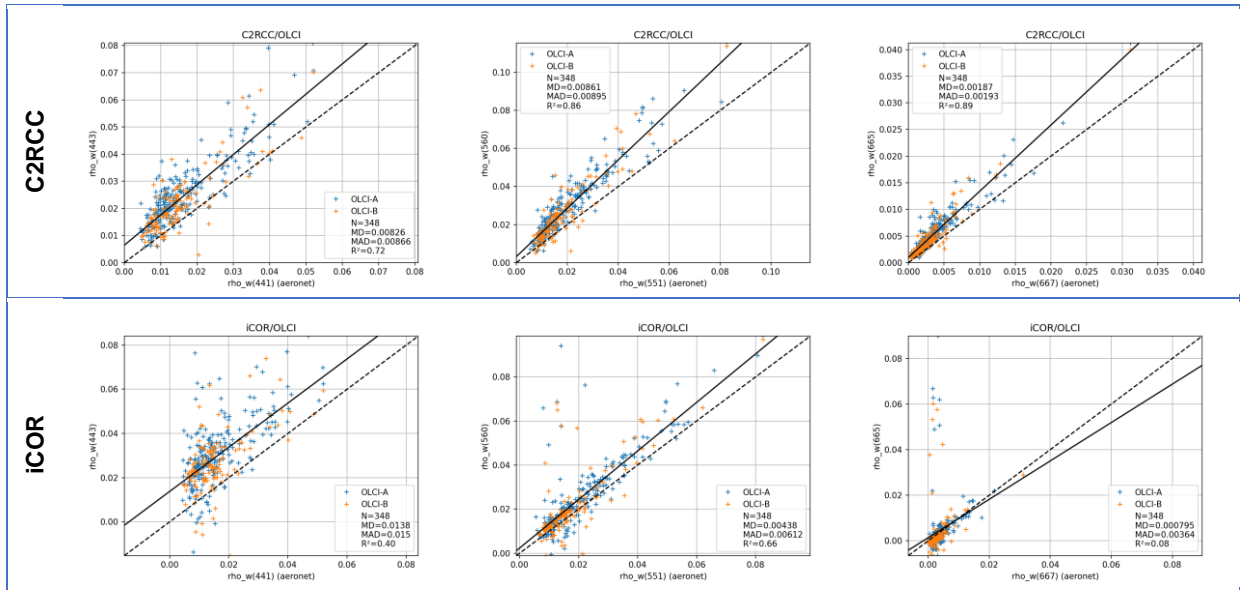
## 6.2.2 Common best quality

### 6.2.2.1 MSI plots



### 6.2.2.2 OLCI plots

### 6.2.2.3 Statistics

| Algorithm | Sensor | N | Mean difference (MD) | | | | | Mean absolute difference (MAD) | | | | |
|---|---|---|---|---|---|---|---|---|---|---|---|---|
| | | | 412nm | 443nm | 490nm | 560nm | 665nm | 412nm | 443nm | 490nm | 560nm | 665nm |
| Polymer | OLCI | 348 | -0.000785 | 0.000235 | -0.00107 | -0.000283 | -0.000137 | 0.00289 | 0.00188 | 0.0019 | 0.00166 | 0.000615 |
| C2RCC | | | 0.005 | 0.00826 | 0.0116 | 0.00861 | 0.00187 | 0.00584 | 0.00866 | 0.012 | 0.00895 | 0.00193 |
| iCOR | | | 0.0191 | 0.0138 | 0.00926 | 0.00438 | 0.000795 | 0.0205 | 0.015 | 0.0105 | 0.00612 | 0.00364 |
| Polymer | MSI | 112 | | -0.000727 | -0.00136 | -0.00178 | 0.000736 | | 0.00291 | 0.00344 | 0.00273 | 0.00113 |
| C2RCC | | | | 0.00474 | 0.00424 | 0.00103 | 0.000407 | | 0.00716 | 0.00708 | 0.00532 | 0.00147 |
| iCOR | | | | 0.00711 | 0.00326 | -0.00126 | -0.000208 | | 0.00875 | 0.0078 | 0.00756 | 0.00634 |
| Acolite | | | | 0.0172 | 0.0145 | 0.0127 | 0.0131 | | 0.0175 | 0.0146 | 0.0129 | 0.0131 |

*Figure 6.4: Statistical values associated with the validation of MSI and OLCI products over the AERONET-OC Venice site in the "common best quality" dataset.*
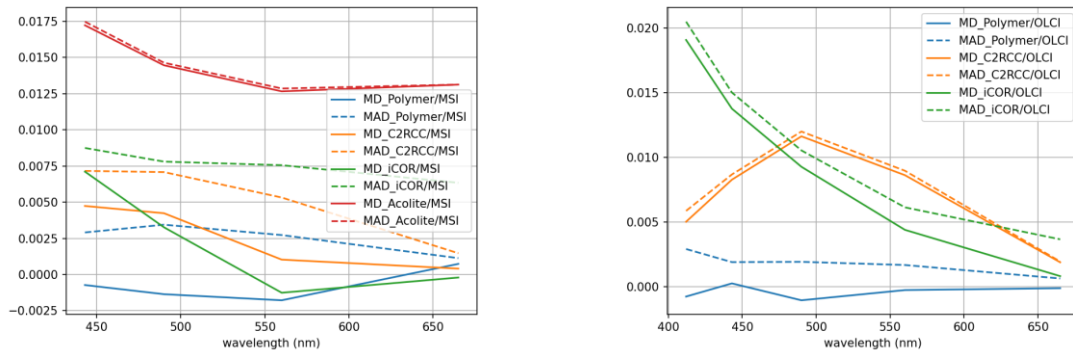


*Figure 6.5: MD and MAD plotted as a function of the wavelength, for each algorithm applied to MSI (left) and OLCI (right) – common best quality*

## 6.3 Discussion

In this exercise, Polymer provided the most accurate results for both MSI and OLCI, with a lower MD and MAD than the other three algorithms. C2RCC has also good results with few outliers. However, a high bias is observed for OLCI with C2RCC, with a maximum bias in the green band (see Fig 6.5). This high bias can be linked with the visual inspection, for which

the atmospheric component for the sample over the gulf of Venice (5.3.6) appears in purple, indicating a possible overestimation of the water reflectance at the green band.

iCOR and ACOLITE are much more sensitive to atmospheric effects, with a large number of outliers in the "individual best quality" dataset, showing that further filtering is required to achieve satisfactory matchups quality. This situation greatly improves with the "common best quality" dataset: the number of outliers is reduced. ACOLITE also shows a large bias, with systematic overestimation of the water reflectance (by more than 0.01 in reflectance across the spectrum). This positive bias is also observed in section 5 (brighter images of ACOLITE water reflectances). This sensitivity to atmospheric contamination makes it difficult to apply iCOR and ACOLITE systematically.

Nevertheless, the Venice site is not sufficiently representative of transitional waters: this validation exercise will be redone with more appropriate in-situ measurements, when available, which will allow monitoring the behaviour of atmospheric correction algorithms in presence of more complex cases encountered in transitional waters: more complex waters, impact from adjacency effects and bathymetry effects.

# 7 Conclusions

The product evaluation presented here had two main purposes:

- Observing the behaviour of each atmospheric correction algorithm on the case study sties of interest, and identify the main characteristics of performance of each one,
- Establishing a procedure to validate the algorithms using in-situ data, starting with AERONET-OC Venice, in view of using further CERTO in-situ data that will be more representative of the transitional waters, which will also allow characterizing the impact of adjacency and bathymetry effects

We have observed that among the considered algorithms, those making assumptions on the spatial variability of the atmospheric properties (scene-based: iCOR and ACOLITE), were the most sensitive to the perturbations by the atmosphere (thin clouds, sun glint – especially since sun glint particularly affect Sentinel-2, see section 4). Furthermore, they do not provide quality flags nor recommendations for flagging, making it difficult to use the products in a systematic way. However, their main strength is to not rely on a model of water reflectance, which makes them well suited over complex or extremely turbid waters.

The pixel-based algorithms (Polymer and C2RCC) are more robust to the atmospheric perturbations and their output contain fewer outliers. However, due to the nature of their design, relying on models for the water and atmospheric reflectances and using the visible bands, modelling errors may lead to imperfect decoupling between the components.

Among those two algorithms, Polymer seems to provide better results, with more consistent decoupling illustrated in section 5, and better performance of the AERONET-OC matchups validation. These results will be consolidated with more specific in-situ data. This report also shows that there is room for possible improvements in Polymer, which are under investigation:

1) The reflectances are underestimated in presence of very highly turbid waters, which has been reported in the frame of CLMS and also [Bi et al. 2018, Renosh et al. 2020]
2) Instabilities in Polymer are observed for OLCI in coastal areas, and are characterized by localized anomalous values. Due to the iterative scheme in Polymer, these

anomalous values are propagated from pixel to pixel. This issue is specific to OLCI, and should be fixable.

# 8 References

Alikas, K., Ansko, I., Vabson, V., Ansper, A., Kangro, K., Uudeberg, K. & Ligi, M. (2020), 'Consistency of radiometric satellite data over lakes and coastal waters with local field measurements', *Remote Sensing* **12**(4), 616.

Bi, S., Li, Y., Wang, Q., Lyu, H., Liu, G., Zheng, Z., Du, C., Mu, M., Xu, J., Lei, S. & Miao, S. (2018), 'Inland water atmospheric correction based on turbidity classification using olci and slstr synergistic observations', *Remote Sensing* **10**(7). http://www.mdpi.com/2072-4292/10/7/1002

Brockmann, C., Doerffer, R., Peters, M., Stelzer, K., Embacher, S., Ruescas & Ana. (2016), Evolution of the c2rcc neural network for sentinel 2 and 3 for the retrieval of ocean colour products in normal and extreme optically complex waters.

Doerffer, R. & Schiller, H. (2007), 'The MERIS case 2 water algorithm', *International Journal of Remote Sensing* **28**(3-4), 517–535.

Keukelaere, L. D., Sterckx, S., Adriaensen, S., Knaeps, E., Reusen, I., Giardino, C., Bresciani, M., Hunter, P., Neil, C., der Zande, D. V. & Vaiciute, D. (2018), 'Atmospheric correction of landsat-8/OLI and sentinel-2/MSI data using iCOR algorithm: validation for coastal and inland waters', *European Journal of Remote Sensing* **51**(1), 525–542.

König, M., Hieronymi, M. & Oppelt, N. (2019), 'Application of sentinel-2 msi in arctic research: Evaluating the performance of atmospheric correction approaches over arctic sea ice', *Frontiers in Earth Science* **7**, 22. https://www.frontiersin.org/article/10.3389/feart.2019.00022

Morel, A. & Gentili, B. (1996), 'Diffuse reflectance of oceanic waters. iii. implication of bidirectionality for the remote-sensing problem', *Applied Optics* **35**(24), 4850–4862.

Pereira-Sandoval, M., Ruescas, A., Urrego, P., Ruiz-Verdú, A., Delegido, J., Tenjo, C., Soria-Perpinyà, X., Vicente, E., Soria, J. & Moreno, J. (2019), 'Evaluation of atmospheric correction algorithms over spanish inland waters for sentinel-2 multi spectral imagery data', *Remote Sensing* **11**(12), 1469.

Renosh, P. R., Doxaran, D., Keukelaere, L. D. & Gossn, J. I. (2020), 'Evaluation of atmospheric correction algorithms for sentinel-2-MSI and sentinel-3-OLCI in highly turbid estuarine waters', *Remote Sensing* **12**(8), 1285.

Steinmetz, F., Deschamps, P.-Y. & Ramon, D. (2011), 'Atmospheric correction in presence of sun glint: application to meris', *Optics Express* **19**(10), 9783–9800.

Steinmetz, F. & Ramon, D. (2018), Sentinel-2 msi and sentinel-3 olci consistent ocean colour products using polymer, *in* 'SPIE Asia-Pacific Remote Sensing proceedings'.

Vanhellemont, Q. (2019), 'Adaptation of the dark spectrum fitting atmospheric correction for aquatic applications of the landsat and sentinel-2 archives', *Remote Sensing of Environment* **225**, 175–192.

Warren, M., Simis, S., Martinez-Vicente, V., Poser, K., Bresciani, M., Alikas, K., Spyrakos, E., Giardino, C. & Ansper, A. (2019), 'Assessment of atmospheric correction

algorithms for the sentinel-2a MultiSpectral imager over coastal and inland waters', *Remote Sensing of Environment* **225**, 267–289.

Zhang, M. & Hu, C. (2020), 'Evaluation of remote sensing reflectance derived from the sentinel-2 multispectral instrument observations using POLYMER atmospheric correction', *IEEE Transactions on Geoscience and Remote Sensing* pp. 1–8.